

Physical Oceanography - UNAM, Mexico

Lecture 1: Introduction to Ocean Circulation

Robin Waldman

August 17th, 2018

Contact :
CNRM, Météo France - CNRS
+33561079336
robin.waldman@meteo.fr

Contents

1	History of a young science	3
1.1	Before the 20th century: scarce observations	3
1.2	First half of the 20th century: first theories	4
1.3	1940's to 1970's: the era of theoreticians	6
1.4	1980's onward: the era of mass observations and numerical modelling	7
1.4.1	Mass observations	7
1.4.2	Numerical modelling	7
1.4.3	Current challenges	11
2	The ocean circulation	15
2.1	Dynamic sea level and its link to circulation	15
2.2	Surface currents	16
2.3	The most visible part of ocean physics: gravity waves	17
3	Ocean hydrography	19
3.1	The most relevant parameter for meteorologists: sea surface temperature	19
3.2	The other ingredient to ocean density: sea surface salinity	19
3.3	Hydrography at depth	20
3.4	The vertical hydrographic structure	22
4	Fluxes at the air-sea interface and climatic relevance	25
4.1	The surface heat fluxes	25
4.1.1	Radiative heat fluxes	25
4.1.2	Turbulent heat fluxes	26
4.1.3	Total net heat flux	28
4.2	The surface momentum fluxes	29
4.3	The surface water fluxes	29
4.4	The oceanic contribution to the Earth's heat balance	29

1 History of a young science

1.1 Before the 20th century: scarce observations

Although humans have been exploring the seas for thousands of years, up to the early 16th century little was known about its circulation owing to the difficulty to measure it. First estimations of surface currents were produced by transatlantic explorers from the measurement of their ships' drift. Indeed, they soon realized that the eastbound return route to Europe could be made shorter by following the Gulf Stream path (Fig. 1.1). Rapidly, good knowledge could be gathered about the main currents and anticyclonic structure of the North Atlantic subtropical gyre. Similar progress would be reached in the 18th century for the North Pacific ocean by whale-hunting navigators.

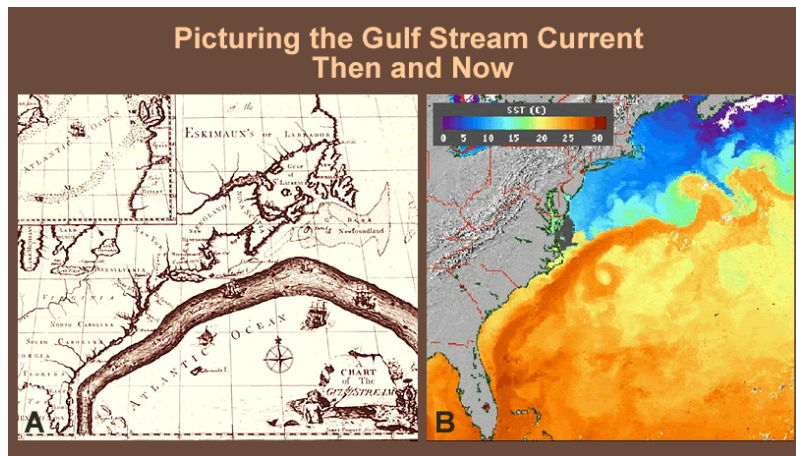


Figure 1.1: (a) Map of the estimated Gulf Stream path by Benjamin Franklin (1770) and (b) a recent satellite image of the Gulf Stream sea surface temperature (source: NOAA). Indeed, sea surface temperature is an excellent indicator of the Gulf Stream's location.

First oceanic thermometers only date back from the 18th century, and they permitted two major discoveries: that the intense Gulf Stream was associated with a strong thermal front (Fig.1.1), and that the deep ocean was very cold even in the Tropics (Fig.1.2). The first discovery is related to the geostrophic balance which holds for most of the large-scale circulation:

$$f\mathbf{k} \times \mathbf{u}_g = -\frac{1}{\rho_0} \nabla_h P$$

with $f = 2\Omega \sin(\phi)$ the Coriolis frequency, \mathbf{k} the vertical unit vector, \mathbf{u}_g geostrophic velocities, ρ_0 the density of seawater and $\nabla_h P$ the horizontal pressure gradient. It states that large-scale pressure gradients are balanced by Coriolis acceleration, so that horizontal velocities can be deduced from the pressure field. This balance was first empirically discovered and formulated for the atmosphere in the 19th century, but it remained unapplicable to the ocean due to the difficulty (still nowadays) to measure oceanic pressure gradients. The second discovery first suggested that intense deep circulations had to occur to bring cold waters from the poles to low latitudes. The observation of cold waters near surface along the equator gave rise to the first schematic of the so-called "thermohaline circulation". It was hypothesized that cold waters were formed and sank at high latitudes, then flew equatorward to resurface at the equator. Only the first two hypotheses turned out to be true.

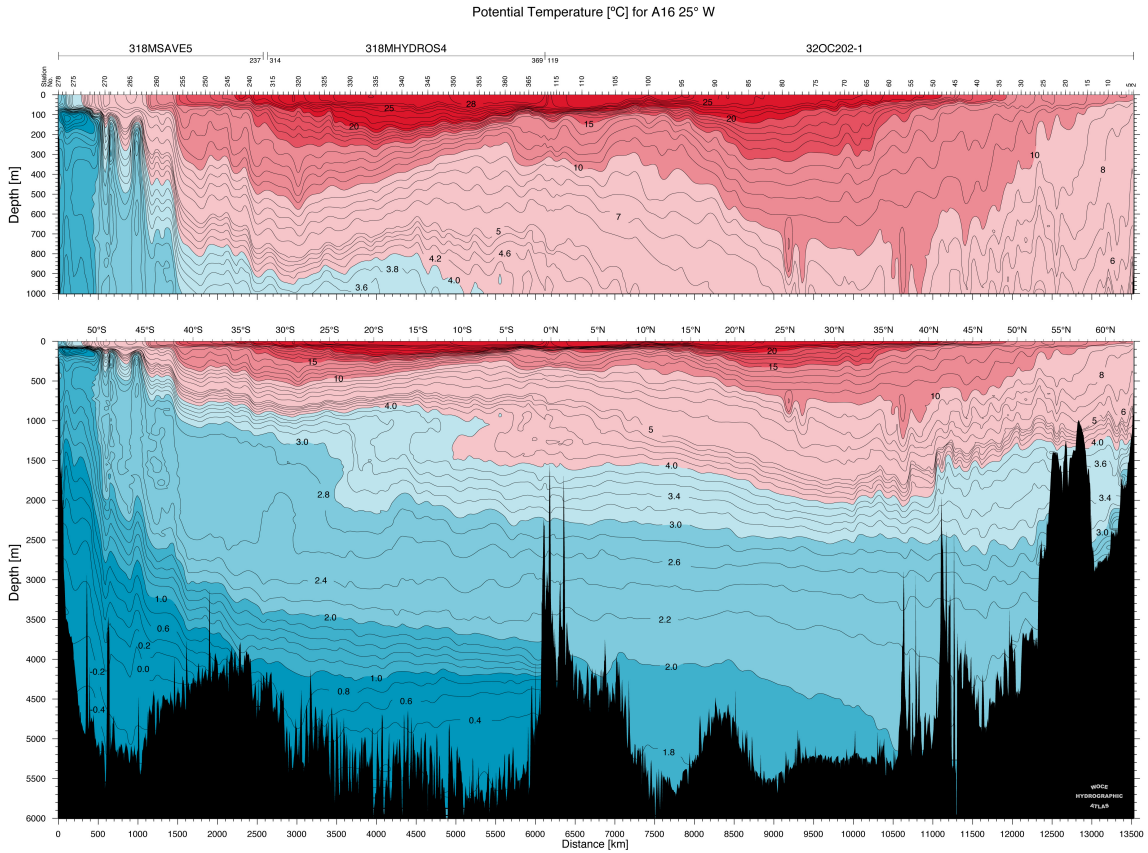


Figure 1.2: Meridional potential temperature section in the Atlantic Ocean (source: World Ocean Database 2013). Below 2000m depth, water masses are colder than 5°C at all latitudes.

1.2 First half of the 20th century: first theories

The geostrophic balance could only be exploited by oceanographers in the early 20th century through the establishment of the "dynamical method" that uses the thermal wind relation. To a very good approximation, the vertical momentum equation is driven by the hydrostatic balance:

$$\partial_z P = -\rho g$$

with $\partial_z P$ the vertical pressure gradient, ρ the in situ density of sea water and g the gravity acceleration. Hence knowledge of density gradients yields the vertical shear of geostrophic velocity through the combination of the geostrophic and hydrostatic balances:

$$\mathbf{k} \times \partial_z \mathbf{u}_g = -\frac{g}{\rho_0 f} \nabla_h \rho$$

This is probably the most useful equation of physical oceanography because of the challenge to directly measure currents, especially at the large-scale. The "dynamical method", routinely used by oceanographers (see Fig.1.3 for an example), consists in retrieving \mathbf{u}_g from the vertical integration of the thermal wind, with the specification of a reference level for the integration (currents either assumed null or estimated at that level).

The Ekman theory is formulated in the same period and gives a first mechanism for the action of wind on ocean currents. Under a series of assumptions (see Chapter 3), it states that over a

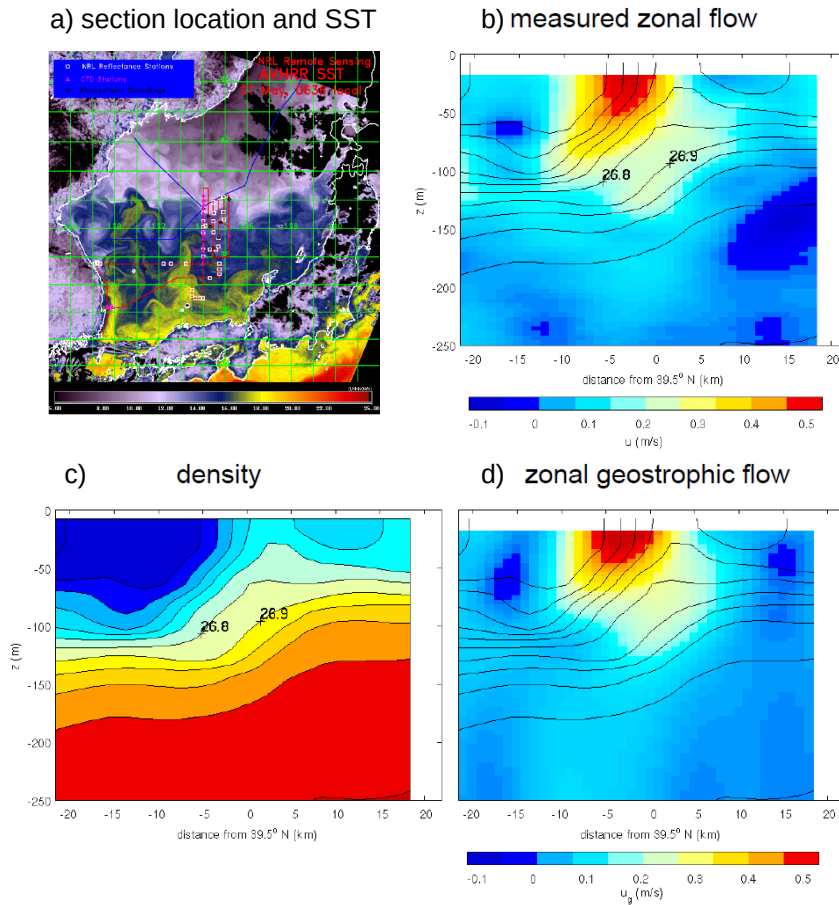


Figure 1.3: Illustration of the validity of the geostrophic relation on the intense North Pacific western boundary current: the Kuroshio. a) Satellite sea surface temperature map and location of the meridional section across the Kuroshio front; b-c) observed in situ zonal velocities and potential density and d) geostrophic velocities deduced from the density section (source: Thomas et al 2010 and Leif Thomas's lectures). Despite the Kuroshio's magnitude and reduced size, it is very well estimated by the geostrophic relation.

wind-driven surface layer, surface wind stress is balanced by the Coriolis acceleration:

$$f\mathbf{k} \times \mathbf{U}_{\text{eh}} = -\frac{1}{\rho_0} \boldsymbol{\tau}_h$$

with \mathbf{U}_{eh} the vertically-integrated horizontal transports and $\boldsymbol{\tau}_h$ the surface horizontal wind stress. Hence, because of the Earth's rotation, the wind stress induces an orthogonal transport to its right in the Northern Hemisphere (to its left in the Southern Hemisphere). This relation explains many features of the surface circulation. At that time, it allowed Ekman to explain why icebergs drifted to the right of the wind in the Northern High Latitudes. Deeper, a second fundamental balance involving the wind stress is established in the 1940's. The Sverdrup balance, involving vorticity dynamics, explains the existence of gyres through the wind stress curl forcing (see Chapter 3). The vorticity of the depth-integrated momentum balance gives, under strong assumptions:

$$\beta V = \mathbf{k} \cdot \nabla_h \times \boldsymbol{\tau}_h = \text{Curl}(\boldsymbol{\tau}_h)$$

with $\beta = \frac{df}{dy}$ the meridional gradient of planetary vorticity and V the vertically-integrated meridional transport. For instance, the subtropical North Atlantic gyre is under negative wind stress curl between the trade winds and the westerly jet, so that Sverdrup theory correctly predicts a southward flow in the interior of the gyre.

Finally, going deeper into the abyssal circulation, a hypothesis is formulated under the deceiving name of the "Sandström theorem", stating that contrary to the atmosphere, the ocean displays a weak deep overturning (or thermohaline) circulation because it is heated from above. Thermodynamically, the cycle described by such a circulation is a "heat engine" that requires a source of mechanical energy to be activated (Fig.1.4). Intense investigations are still ongoing to identify this source of energy.

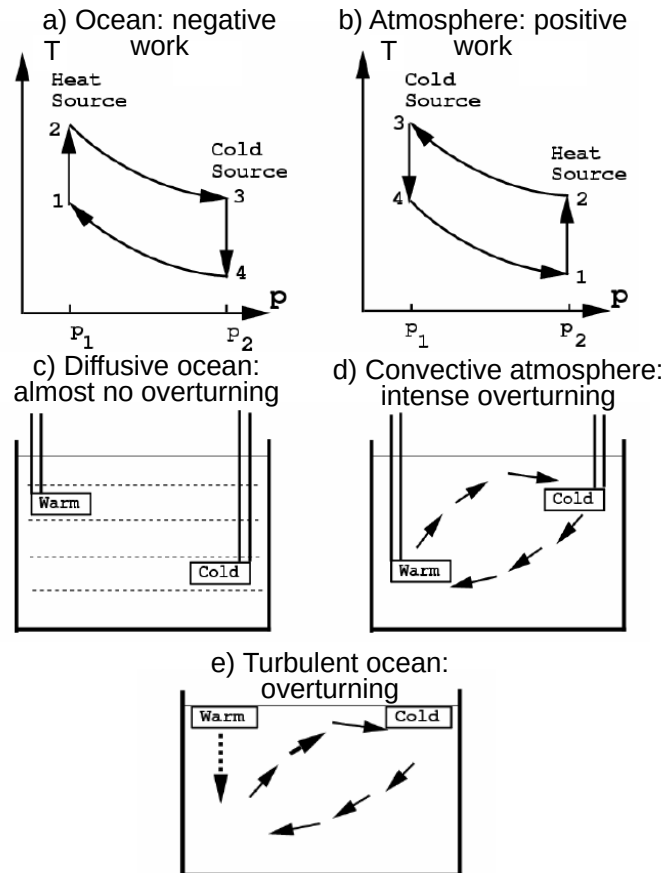


Figure 1.4: Illustration of Sandström's "theorem": (adapted from Haosheng Huang's lectures). a) The ocean heat engine produces negative work because it is heated at low pressure and cooled at higher pressure, b) contrary to the atmosphere. c) Hence if it were purely diffusive, it would have almost no vertical overturning, d) contrary to the convective atmosphere heated from below. e) Turbulent vertical mixing is required to transfer the surface heating to deep layers so that the ocean can feature an overturning circulation.

1.3 1940's to 1970's: the era of theoreticians

In the mid-20th century, following Sverdrup's work and the rapid development of dynamic meteorology, a series of theories are proposed that try to explain the general structure of oceanic gyres, and in particular their western intensification. The first models that close the gyre circulation are proposed by Stommel and Munk (see Chapter 3). They assume an ocean with constant density on a rectangular basin, and they succeed to represent intensified western boundary currents by accounting the ocean interaction with the basin boundaries (either bottom or lateral). It is worth also mentioning fundamental theoretical developments regarding the role of topography on the general circulation, the development of baroclinic and barotropic instabilities and the formulation of turbulence models to understand the presence of a well-mixed surface boundary layer called the

oceanic "mixed layer".

1.4 1980's onward: the era of mass observations and numerical modelling

Until very recently, most of the knowledge regarding ocean circulation was hypotheses or mere speculations due to the lack of observations and the poor numerical computation capacities. This is why even well-established balances such as the Sverdrup relation have fairly limited domains of validity (see Chapter 3).

1.4.1 Mass observations

Recently, the development of satellite observations, mostly sea surface temperature (from the 1970's) and dynamic sea level retrievals (from the 1990's), and the generalization of in situ hydrographic measurements with the ARGO network (from the 2000's) have revolutioned the way we understand oceanic circulation. Although sea surface temperature (SST) has long been the easiest measurable oceanic physical parameter, its satellite estimation from infrared measurements has given a global high-resolution picture of it (Fig.1.5a). It has allowed to identify the ubiquity of mesoscale eddies and even smaller-scale fronts and filaments, and it is a major means to estimate global SST trends. However, satellites only measure the temperature of a cold skin layer located within the surface $\sim 10\mu m$, so that a systematic cold bias is present when compared to surface in situ measurements performed typically at $\sim 1m$ depth. The second and more revolutionary satellite measurement has been the dynamic sea level estimation (Fig.1.5b), defined as the height of the sea surface with respect to the geoid (the gravity equipotential surface). The dynamic sea level relates to ocean surface dynamics and constitutes by far the main dynamical observation assimilated by ocean forecast centers, which explains why many of them only produce reanalyses from the satellite altimetry era onward. Satellite altimetry has allowed to quantify the oceanic general circulation, but most significantly it has revealed the ubiquity and domination of mesoscale eddies in ocean dynamics. It is also a high-impact parameter for vulnerable coastal populations under the threat of sea level rise.

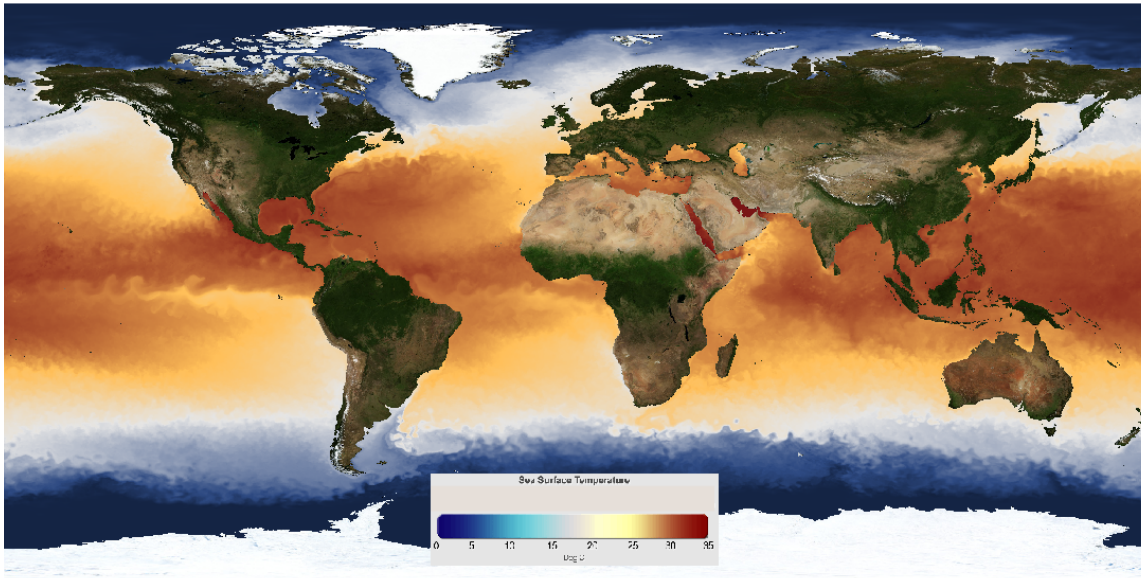
In the 2000's, the ARGO program has aimed at observing simultaneously the hydrographic properties of the global ocean with autonomous drifts (Fig.1.6). It has dramatically increased the spatial coverage of the upper 2000m layer. Thanks to this ongoing program, we have largely improved the measurement of oceanic heat content trends, the climatology of poorly-observed regions (e.g.: the Southern Ocean), the mixed layer depth distribution and vertically-integrated oceanic transport estimations through the knowledge of ARGO floats drift at their parking depth $\sim 1000m$.

Lately, novel means of in situ oceanic observations have been developed, avoiding the large cost of a ship campaign but capable to glide autonomously. These so-called "gliders" are being launched to perform repeated hydrographic sections that estimate transports, and to characterize the intense meso and submesoscale oceanic activity (Fig.1.7).

1.4.2 Numerical modelling

Simultaneously and thanks to the explosion of observational oceanography, the revolution of numerical modelling has allowed to represent realistically the ocean circulation and to produce ocean forecasts and climate change scenarios. The oceanic resolution depends on the specific constraints and questions addressed, but it ranges typically from $\sim 1^\circ$ for global climate applications to

a) Sea surface temperature



b) Dynamic sea level

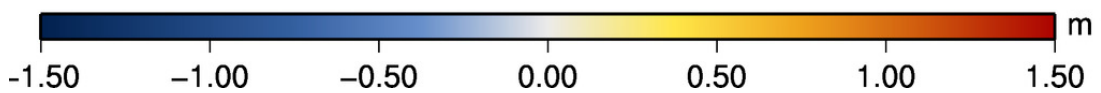
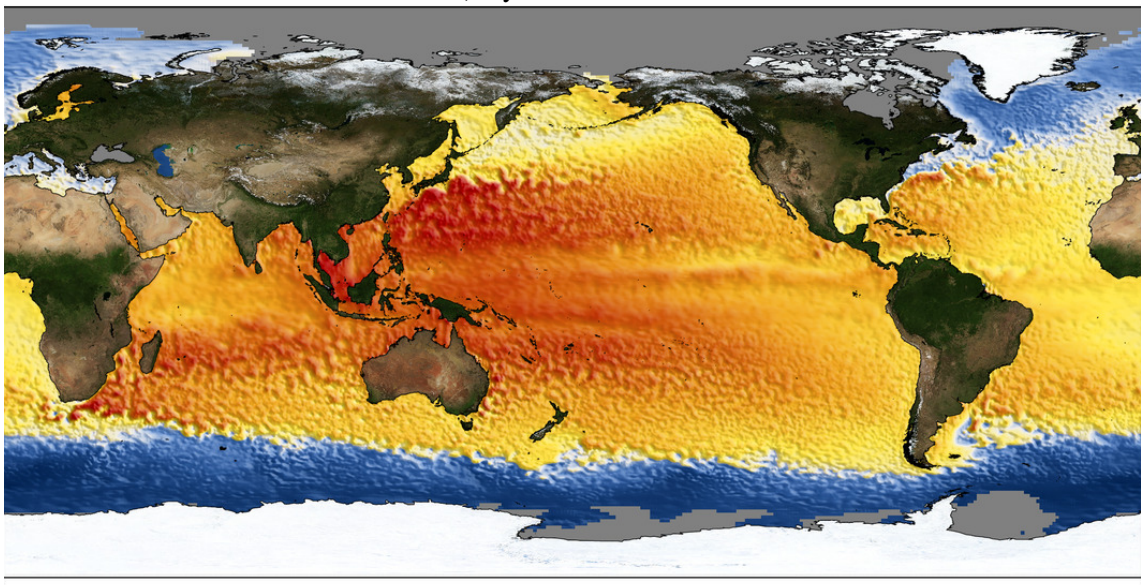


Figure 1.5: a) Near real-time sea surface temperature analysis on Aug. 29th 2018 assimilating mostly satellite observations (source: NOAA). b) Daily gridded dynamic sea surface height on Dec. 31th 2012 retrieved from satellite (source: AVISO). Satellite observations give an accurate and high-resolution picture of surface circulation and heat content. General circulation patterns as well as intense fronts and mesoscale turbulence are visible.

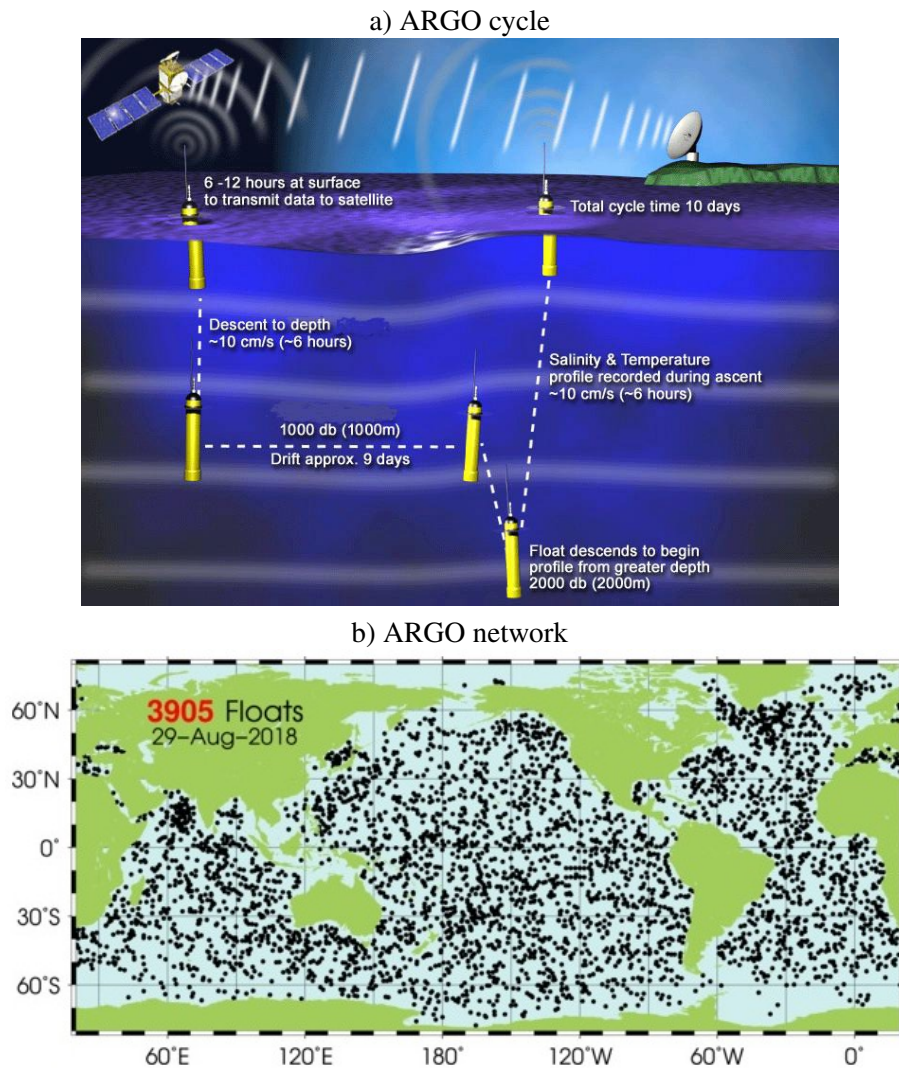


Figure 1.6: a) Functioning of an ARGO float and b) the ARGO network on a given day (source: ARGO database). Main strengths: the coverage is global and it gives both the in situ profile and an estimated velocity at the parking depth.

$\sim 1/10^\circ$ for ocean-only regional studies and $\sim 1/100^\circ$ for coastal applications. We can distinguish several ocean modelling frameworks, each one with specific applications:

- Operational oceanography, both at coastal and global scales, assimilates observations in numerical models to produce oceanic forecasts (Fig.1.8). Data assimilation is a core aspect of their activity.
- So-called "coupled physical-biogeochemical" models aim at representing biogeochemical cycles of matter (e.g. C, N, P), the distribution of nutrients and the dynamics of biological populations (from plankton to fish), either for ecological or fisheries applications (Fig.1.9). They add to the physical ocean model a biogeochemical module which is forced by the former, but in most case does not force the physics so that it is improper to refer to "coupling".
- Coupled ocean-atmosphere models can be used from operational weather forecasts to long-term climate projections, including sub/seasonal and decadal forecasts (Fig.1.10). They usually also include a continental surface model and can include an atmospheric chemistry module. Due to the short atmospheric memory, ocean-atmosphere coupling is compulsory

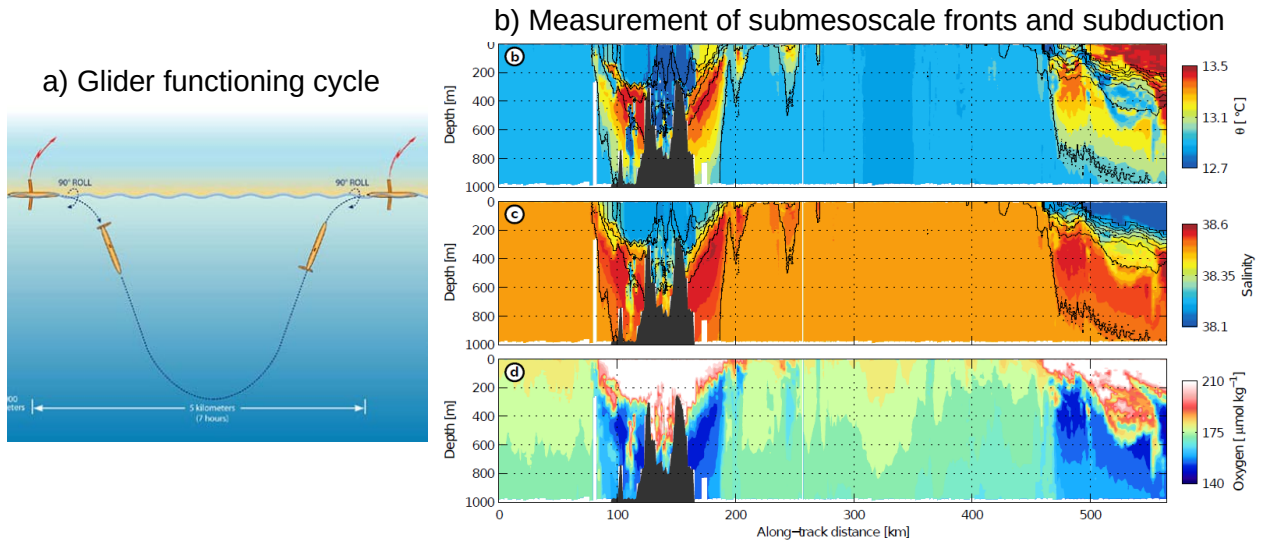


Figure 1.7: a) Functioning of a glider and example of a b) potential temperature, c) salinity and d) oxygen concentration section across several fronts in the Mediterranean Sea (source: Anthony Bosse's PhD thesis). Main strengths: autonomous drift and small-scale in situ observations.

for seasonal scales and beyond. For shorter scales, coupling matters for high-frequency phenomena with strong air-sea feedbacks, such as tropical cyclones or sea ice dynamics.

- So-called "Earth System Models" are climate models that include, in addition to the ocean-atmosphere coupling, a representation of the carbon cycle which can freely feedback on climate.

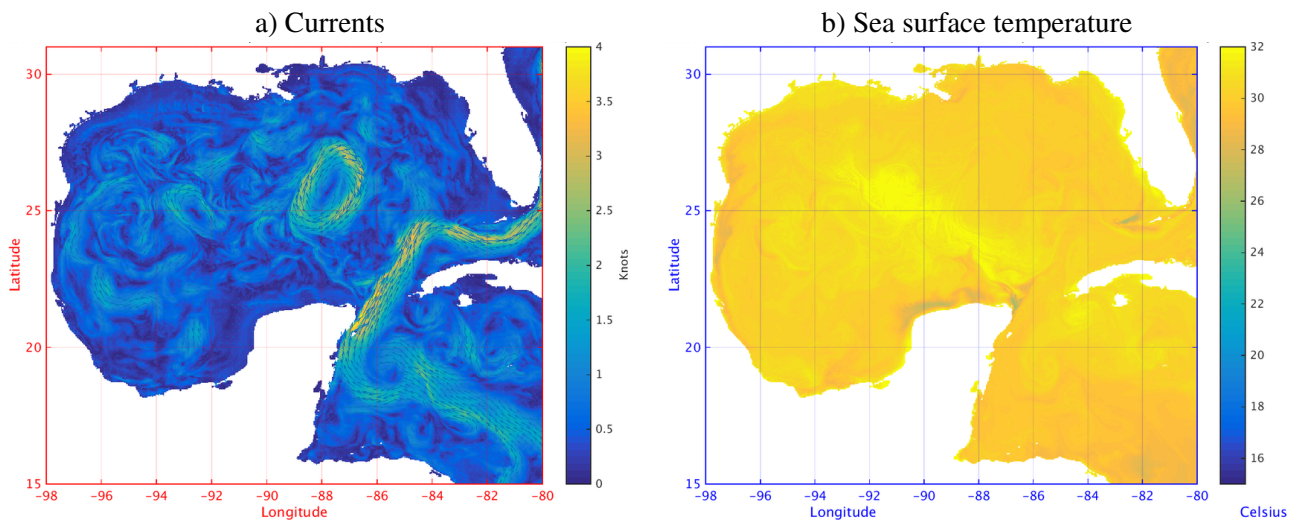


Figure 1.8: 4th day surface ocean forecast on Sep. 2nd 2018 for the Gulf of Mexico (source: NOAA). Largest velocities are part of the western boundary current of the subtropical gyre (here the "Loop Current"). The circulation is highly turbulent with numerous mesoscale eddies and the northern Yucatán upwelling has a sea surface temperature signature.

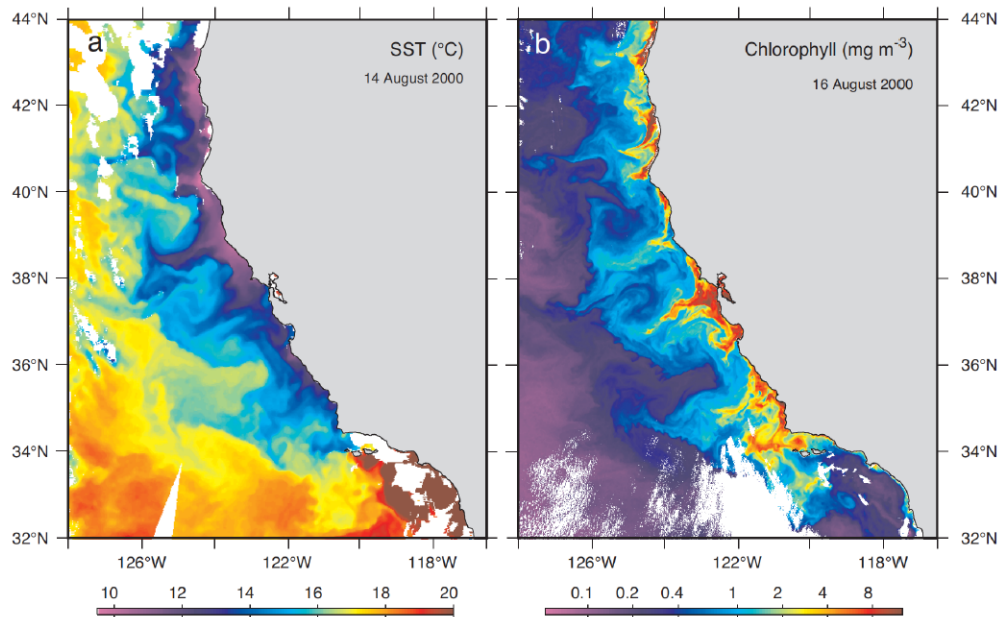


Figure 1.9: Satellite maps of sea surface temperature and surface chlorophyll concentration off the US West Coast (source: Sarmiento and Gruber 2006). Biological activity is very sensitive to ocean physics, and in particular to vertical exchanges.

1.4.3 Current challenges

Despite its recent spectacular developments, physical oceanography is still a young science, which is great news for young scientists! Regarding observations, we can stress some of the major limitations of the current instrumental networks.

- Most in situ observations, including ARGO measurements, are performed above 2000m depth, hence covering less than half of the oceanic volume (Fig.1.11a). Most is still unknown about the abyssal circulation, and in particular how vertical motions and mixing occur and how they contribute to global warming.
- In situ observations of dissipation and its relation to mixing are scarce, generally very localized in time and space (Fig.1.11c). Hence large uncertainties exist regarding the magnitude and the processes governing water mass transformations.
- Most velocity estimations are indirect, either from thermal wind or from floats' drifts. Current-meters are scarce, even along the best documented currents.
- The heat budget of individual basins still remains very uncertain, so that the ocean causes the largest error in the climate system warming trend estimations (Fig.1.11b). This is due to the lack of continuous arrays documenting heat transports across basins.
- Despite their key role for climate, air-sea fluxes are very poorly known, especially the turbulent sensible and latent heat fluxes. So that existing air-sea flux climatologies are usually far from closing the global heat and water budgets at the air-sea interface.

As for ocean modelling, the main limitations are posed by the above-mentioned poorly known processes and numerical computation limits.

- Among the poorly represented processes, it is worth mentioning the poor physics related to mixing in the interior ocean (below the mixed layer) and the large uncertainties around the

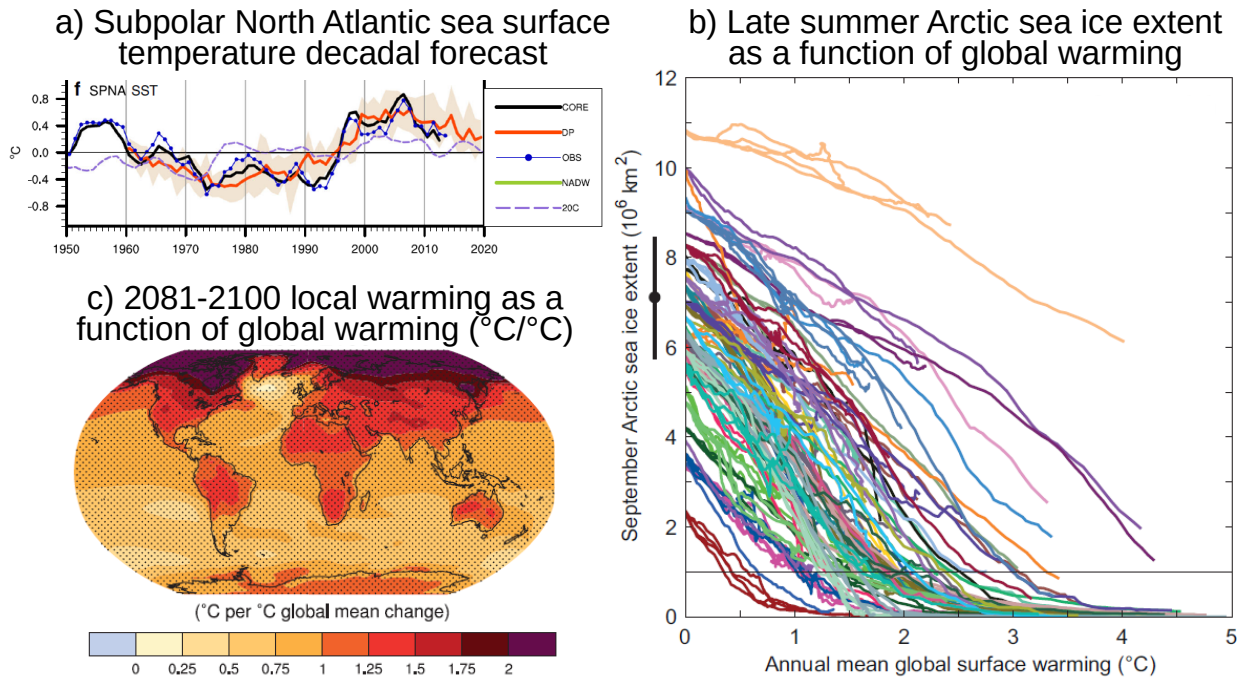


Figure 1.10: Climate applications of ocean modelling: a) decadal prediction of sea surface temperature in the Subpolar North Atlantic (source: Yeager et al 2017), b) climate scenario of the late summer Arctic sea ice extent as a function of global warming and c) 2081-2100 local warming as a function of global warming (source: IPCC AR5, 2013). Decadal predictions present some skill in the ocean (compare the red and dashed purple lines). Climate scenarios indicate that warming should be reduced above the ocean except in the Arctic where the summer sea ice is likely to disappear completely by 2100 (colors indicate different climate models and the horizontal black line indicates a nearly ice-free Arctic).

formulation of air-sea fluxes.

- The ocean is a highly-turbulent fluid that requires resolving millimetric to global scales. This will clearly remain impossible for a long time, and currently ocean models miss most turbulent scales. Quasi-geostrophic mesoscale eddies are barely represented in large-scale configurations, but in most cases they must be parametrized. This is a large source of error as mesoscale eddies are the most energetic features of ocean circulation (Fig.1.12).

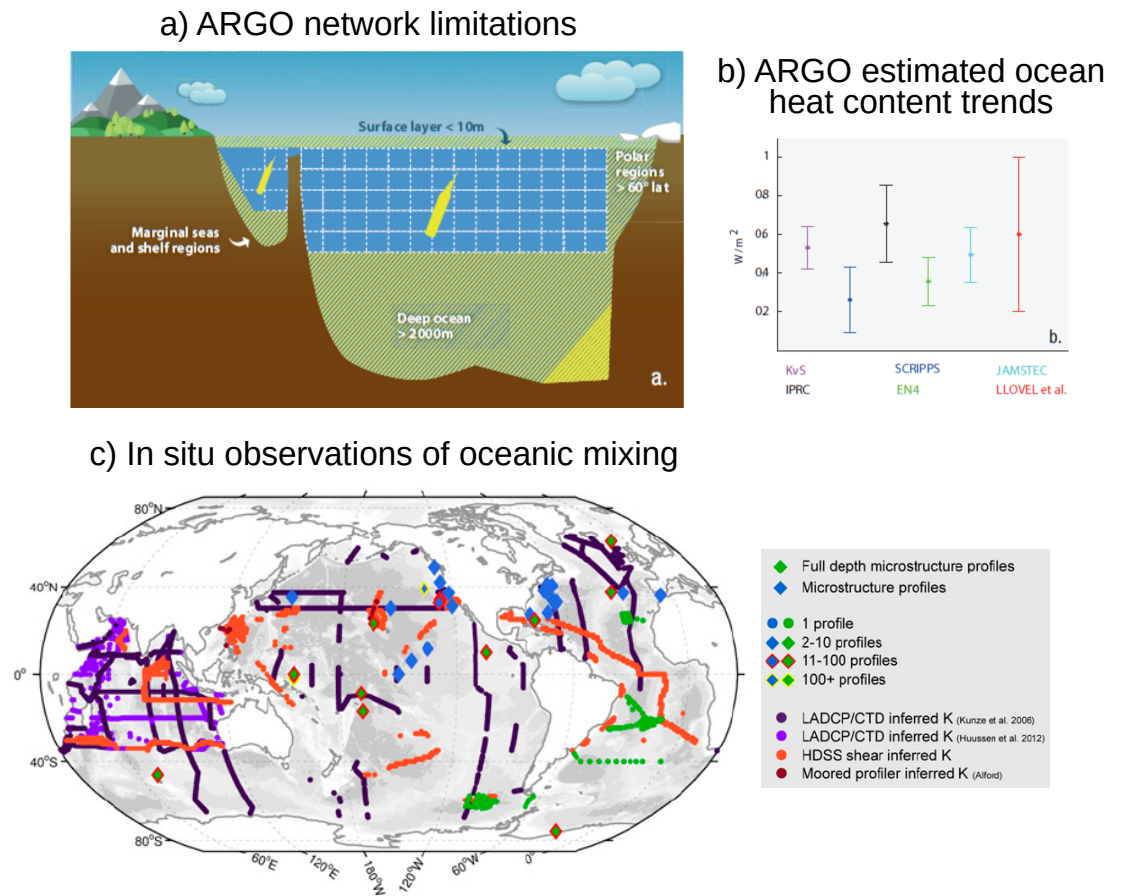


Figure 1.11: a) Illustrations of the main ARGO network limitations and b) consequence for the 2006-2012 heat content trend of the upper 2000m estimated by different institutes (source: von Schuckmann et al 2016). c) Location of in situ observations of oceanic mixing (source: Waterhouse et al 2014). In situ observations still cover a minority of the oceanic volume, hence the large errors on the estimation of ocean warming. Mixing measurements are very scarce in space and time.

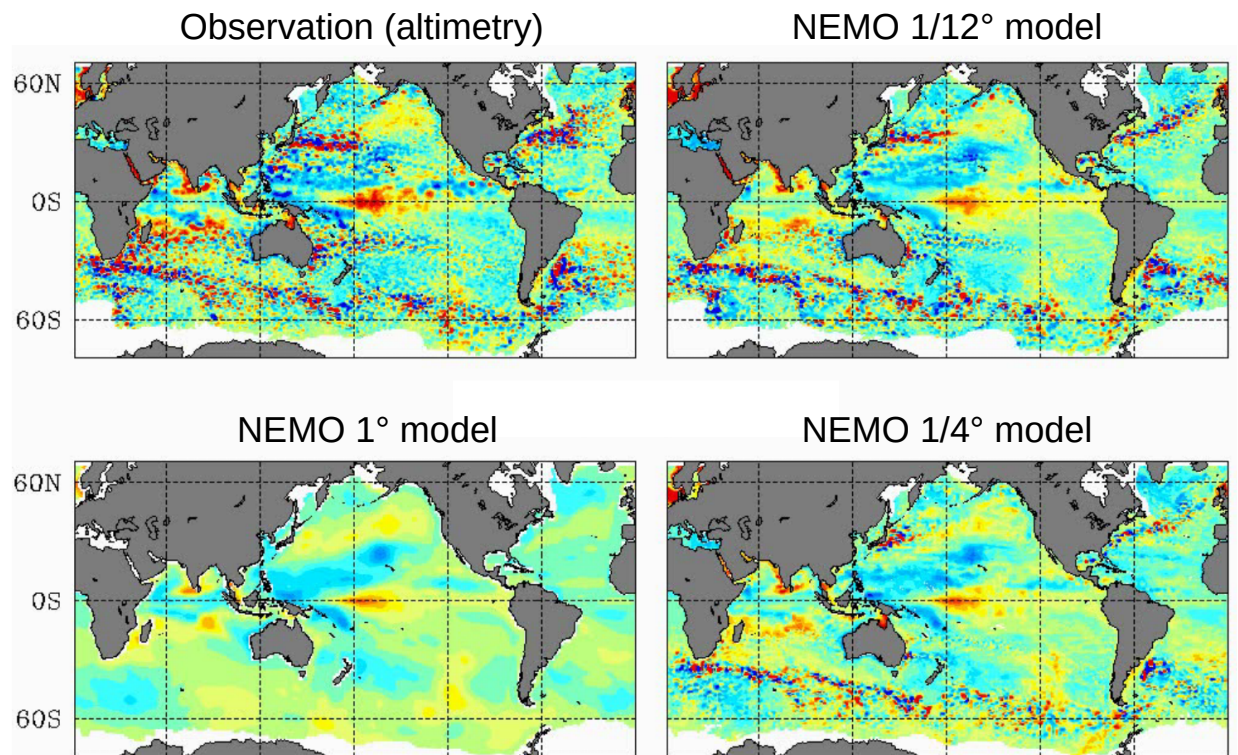


Figure 1.12: Illustration of the challenge related to horizontal model resolution (source: Bernard Barnier's lecture). Comparison of a daily sea level anomaly field on Jan. 6th 1993 retrieved from observations, a typical short-scale ocean model (NEMO 1/12°), its climate counterpart (NEMO 1°) and an intermediate resolution (NEMO 1/4°). The climate ocean model misses most surface circulation, which is related to mesoscale eddies.

2 The ocean circulation

2.1 Dynamic sea level and its link to circulation

As mentioned before, the main observation of oceanic currents is indirect and comes from satellite altimetry. Indeed, sea surface height η is directly related to surface geostrophic velocities through the geostrophic and hydrostatic relations:

$$f\mathbf{k} \times \mathbf{u}_{g0} = -\frac{1}{\rho_0} \nabla_h P = -g \nabla_h \eta$$

so that except along the Equator, sea level isolines are streamlines of surface geostrophic currents. To a very good approximation, the sea level pressure gradients can be neglected. The most visible features of this surface circulation (Fig.2.1) are: Western-intensified subtropical gyres (positive η , hence anticyclonic circulation) and subpolar gyres (negative η , hence cyclonic circulation), an intense and meandering westerly Antarctic Circumpolar Current. In a very narrow band along the Equator, the geostrophic balance breaks down so that zonal sea level gradients must be balanced: the pressure force would push waters eastward, hence an equal and opposite force must push them westward.

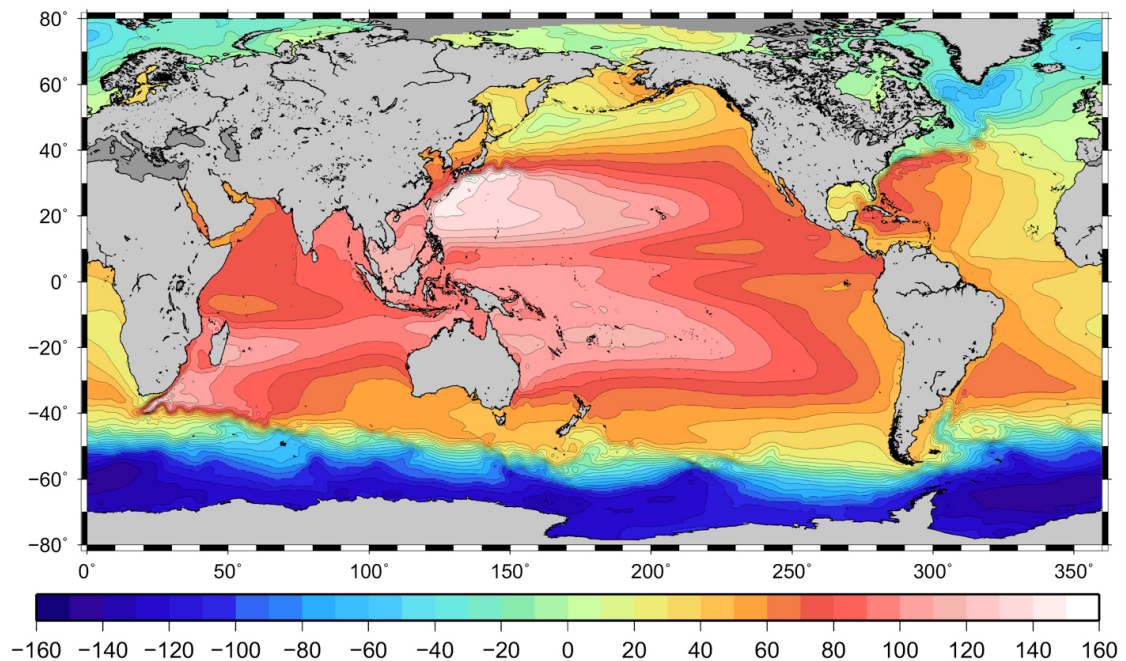


Figure 2.1: Mean dynamic topography (cm) deduced from satellite (source: ESA/CNES/CLS). Gyres and the Antarctic Circumpolar Current stand out most clearly.

The average dynamic sea level differs largely from its instantaneous picture (see Fig.1.12), so much that many average circulation features are not visible anymore in a daily to monthly-mean map. Indeed, the average flow is a weak residual from a very intense transient eddy flow. Oceanic eddies are ubiquitous: several thousands of them can be detected by altimetry at any given time. They are particularly intense and numerous along the most energetic mean currents: Western Boundary Currents and the Antarctic Circumpolar Current. Those eddies have a typical scale of $L \sim 100km$, hence they are named mesoscale eddies although their dynamics are quasi-geostrophic and similar to synoptic atmospheric eddies. Similarly to the atmosphere, they scale with the (first)

Rossby radius of deformation R_d which measures the horizontal scale of geostrophic adjustment of any oceanic perturbation.

Exercise: estimate the typical oceanic Rossby radius of deformation. Predict how it evolves with latitude. Definitions: $R_d = \frac{NH}{\pi f}$ with $N = \sqrt{-\frac{g}{\rho_0} \partial_z \rho}$ the Brunt-Vaisala frequency, $H \sim 5000m$ the ocean depth, $f \sim 10^{-4} s^{-1}$ at mid-latitudes, $\rho_0 = 1026 kg/m^3$ the average density of sea water and a typical vertical stratification $\partial_z \rho$ of $-5 kg/m^3$ over the depth H .

Solution: estimated $R_d \sim 50km$ at mid-latitudes, which compares well with the observed surface eddy field. We note however that mesoscale eddies are usually larger than R_d , due to their merging by the inverse cascade of quasi-geostrophic turbulence. R_d decreases with increasing latitude and decreasing vertical stratification, both contributing to a reduced eddy size at high latitudes. R_d can reach typically $5km$ at high latitude, which is a major challenge of physical oceanography because of the key role of mesoscale eddies in the circulation.

Finally, although η is only a measure of surface currents, it is directly related to the vertically-integrated (barotropic) transport in the case of a barotropic ocean, with a constant density ρ_0 . Indeed, in that case:

$$\mathbf{k} \times \mathbf{U}_g = \mathbf{k} \times \int_{-H}^0 \mathbf{u}_g dz = \frac{g}{f} \int_{-H}^0 \nabla_h \eta dz = \frac{gH}{f} \nabla_h \eta = H \mathbf{k} \times \mathbf{u}_{g0}$$

This means that η is the streamfunction of the vertically-integrated geostrophic transport \mathbf{U}_g in a barotropic ocean, this transport being equal to \mathbf{u}_{g0} times the ocean depth H . However, the ocean is far from being barotropic and velocities generally cancel at depth. Nevertheless, η gives a good qualitative view of the barotropic circulation because surface currents dominate the vertically-integrated transport.

2.2 Surface currents

Surface currents are not directly measurable from satellite, but they can be simulated by numerical models (Fig.2.2). They give a very similar picture to altimetry, with additional elements regarding equatorial, wind-driven and less energetic circulations. Equatorial currents are actually the most energetic ones of the global ocean, and they flow generally westward. They are pushed by Easterlies and intensified by the absence of Coriolis acceleration along the Equator. Water masses are packed at the western boundary, which explains the positive sea level anomaly there.

Outside of the Equatorial band, currents are mostly at geostrophic balance, with most of their energy at the mesoscale. However, we note large-scale Ekman currents directly forced by the wind stress. Finally, we note that intense currents have a typical magnitude of $\sim 1m/s$, and weaker ones fall down to $\sim 10cm/s$. Among them are equatorward-flowing eastern boundary currents at the subtropical latitudes, which are as we will see the geostrophic response to coastal upwelling.

Exercise: from the typical horizontal length and velocity scales of oceanic motion, estimate the time scale of the oceanic circulation and compare it to the atmosphere.

Solution: $T \sim 1$ year in the ocean versus $T \sim 1$ week in the atmosphere. Hence relative decoupling between both fluids: the ocean is felt as a relatively constant surface for atmospheric motions, and the atmosphere is felt as stochastic noise for oceanic motion. Thus although ocean circulation theory mostly focuses on the wind forcing, this driving force is not straightforward. A notable exception to this decoupling is in the Tropics where the oceanic response is quicker and air-sea fluxes are more intense.

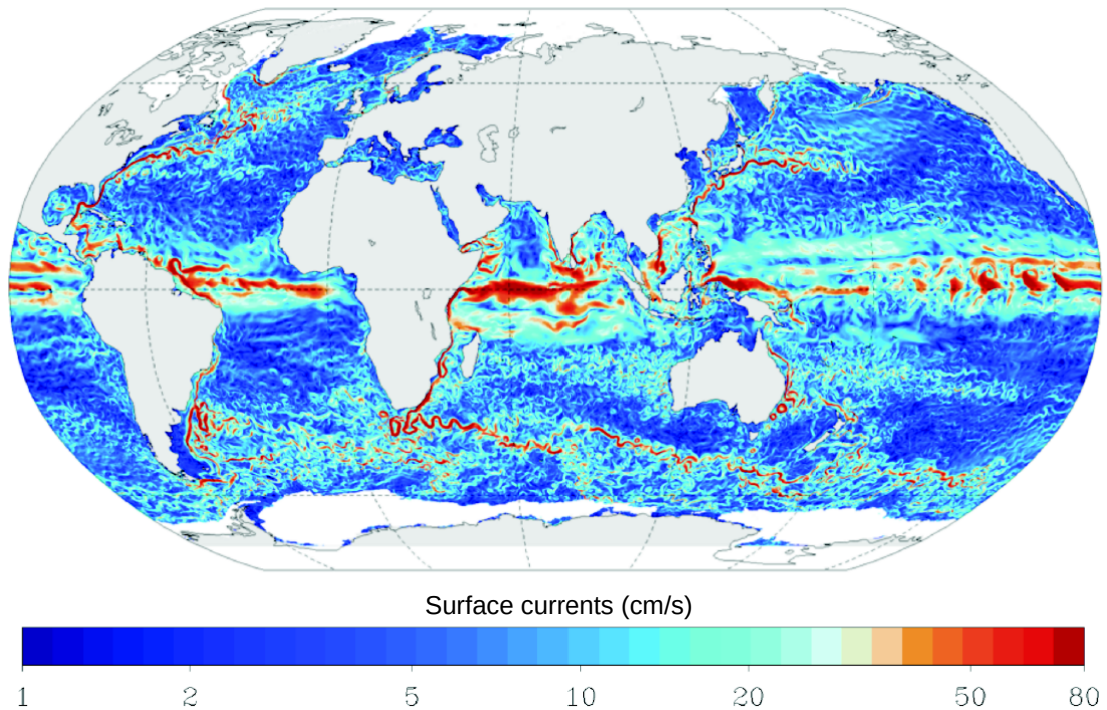


Figure 2.2: Snapshot of surface currents in a $1/12^\circ$ resolution ocean simulation (source: Tréguier et al 2017). In addition to Western Boundary Currents and the Antarctic Circumpolar Current, intense equatorial currents and mesoscale eddies stand out.

2.3 The most visible part of ocean physics: gravity waves

Although gravity waves such as tides and wind waves are the main oceanic physical property that humans can witness with the eye, they mostly have an indirect effect on the large-scale circulation. Hence they are usually not explicitly represented in ocean circulation models but considered as external forcings for the circulation. Tides and wind waves impact the circulation and water mass properties by inducing mixing when they break, or by modulating the surface ocean roughness and hence air-sea fluxes. Although mixing by gravity waves has been postulated as a key mechanical energy source for the ocean thermohaline circulation, many unknowns remain about its magnitude and underlying physics.

Under the action of the Moon and Sun's gravitational forces, the barotropic (or external) tide is set into motion in the ocean. Most of it ($\sim 70 - 80\%$) is dissipated above shallow continental margins by bottom friction resulting in local mixing. However a significant fraction is converted into baroclinic (or internal) tides through its interaction with topography (Fig.2.3 and Fig.2.4). This interaction is very complex but a large fraction of those waves are trapped and dissipate locally, hence generating mixing near topography. The remaining radiates and dissipates elsewhere. Overall, tidal dissipation generates enhanced mixing near the topography, especially above mid-ocean ridges, continental shelves and rough abyssal plains, which modifies water mass density and hence modulates oceanic currents.

Under the action of winds, both external and internal gravity waves are generated, which also contribute to mixing when they break. Their generation and hence dissipation is enhanced at mid-latitudes where most intense surface winds are located (Fig.2.4). External waves are named wind wave when they are in balance with the overlying wind or swell when they were generated elsewhere. They can increase the surface ocean roughness, which intensifies turbulent air-sea

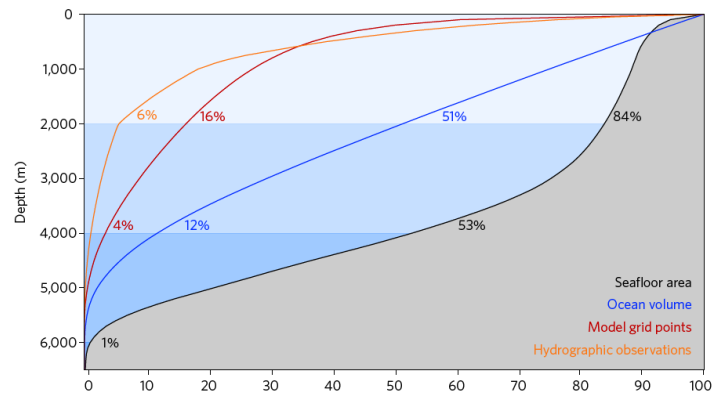


Figure 2.3: On the importance of the seafloor distribution for the ocean ventilation (source: de Lavergne et al 2016). Abyssal oceans concentrate most of the interaction with topography but are by far the least observed and modelled regions.

fluxes of heat, momentum and water. Their breaking is a surface source of turbulent kinetic energy which enhances surface mixing within the mixed layer. As for internal waves, they are generated by near-inertial motions in the mixed layer under the action of surface winds. A fraction of them locally dissipate and also contribute to mixing in the mixed layer, whereas the remaining are radiated below and dissipate at distance.

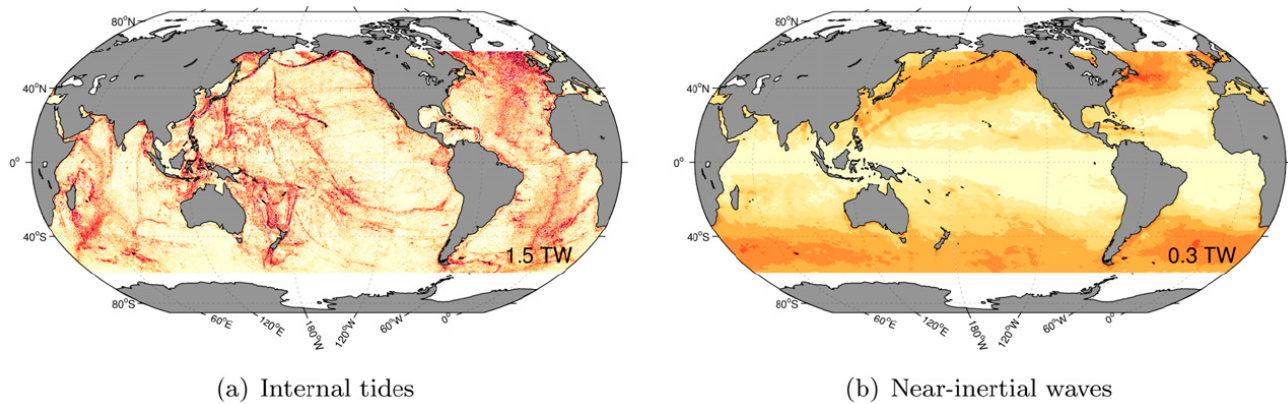


Figure 2.4: Contrasting locations for the generation of internal tides and wind (or near-inertial) waves (source: Waterhouse et al 2014). The former are formed near topography whereas the latter develop below the intense mid-latitude Westerly winds.

3 Ocean hydrography

3.1 The most relevant parameter for meteorologists: sea surface temperature

The sea surface temperature (SST) is the main oceanic regulator of air-sea exchanges, so that still nowadays it is the main (if not the only) oceanic focus of atmospheric scientists. This includes water exchanges, and because the ocean is the main water provider to the atmosphere, a famous meteorologist used to tell his students: "Meteorologists consider the ocean as a wet surface." However, SST patterns are strongly regulated by ocean dynamics which redistributes heat, and that is why ocean circulation should also matter for meteorologists.

The global average SST map (Fig.3.1) shows the expected meridional gradient between warm tropical and cold polar waters. However, an intense zonal gradient appears at most latitude, with warmer waters to the west in the Tropics and reversely at high latitudes. This is consistent with the gyre circulation with poleward-flowing western boundary currents at subtropical latitudes and equatorward boundary currents at subpolar latitudes. In addition, intense cold anomalies are visible at the eastern edges of subtropical basins, consistently with the presence of wind-driven upwelling. Finally equatorial regions are separated in all basins between an eastern "cold tongue" and a western "warm pool", which is consistent with intense westward currents pushed by trade winds. The warm water is packed to the west, whereas to the east intense upwelling brings cold water from below to the surface.

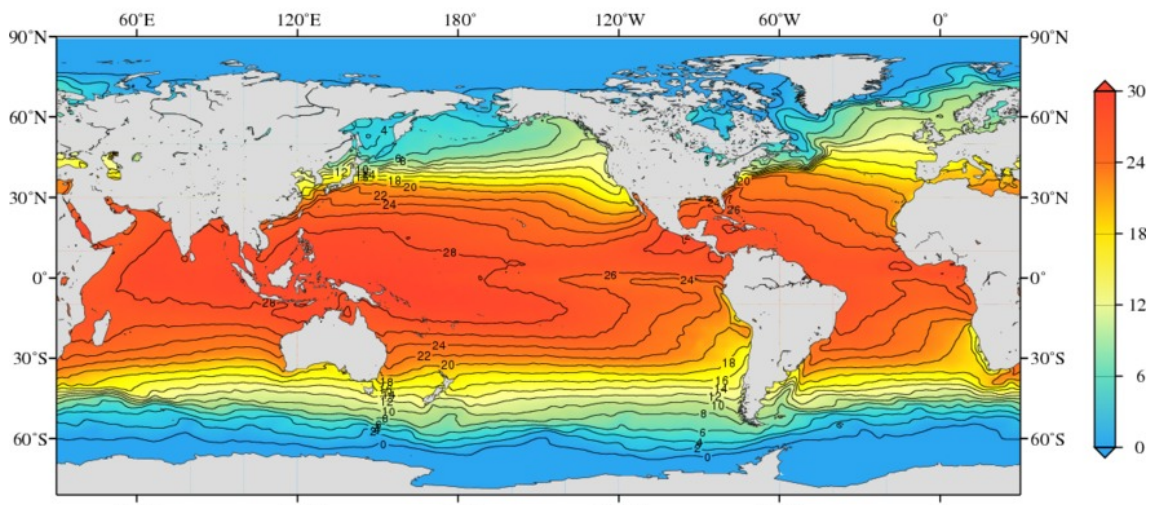


Figure 3.1: 1955-2012 mean sea surface temperature in °C (source: World Ocean Atlas). Strong circulation-related zonal gradients appear in addition to the expected meridional gradient.

3.2 The other ingredient to ocean density: sea surface salinity

The oceanic density is determined by both its temperature and salinity, that is its concentration of dissolved salts in $g/kg = ‰$. Hence salinity is also an active tracer impacting ocean circulation through its modulation of density, and hence of the pressure gradient force in the momentum balance. The global average distribution of sea surface salinity (SSS, Fig.3.2) describes, to a certain

extent, the surface water budget between evaporation and precipitation. In particular, the excess of precipitation over evaporation in the deep Tropics along the Inter-Tropical Convergence Zone (ITCZ) and at high-latitudes causes low SSS. On the contrary, at subtropical latitudes, evaporation exceeds precipitation, which causes high SSS. We also identify the surface signature of the main river plumes whose runoff is the third main component of the ocean water budget. There is also a basin-scale imbalance between a fresher Pacific and a saltier Atlantic Ocean, which is explained by the larger precipitation over the Pacific than the Atlantic. Finally, we also identify signatures of the circulation: the fresher eastern Equatorial and subtropical areas are related to the upwelling of deeper waters, which are generally fresher than at surface as it will be shown soon.

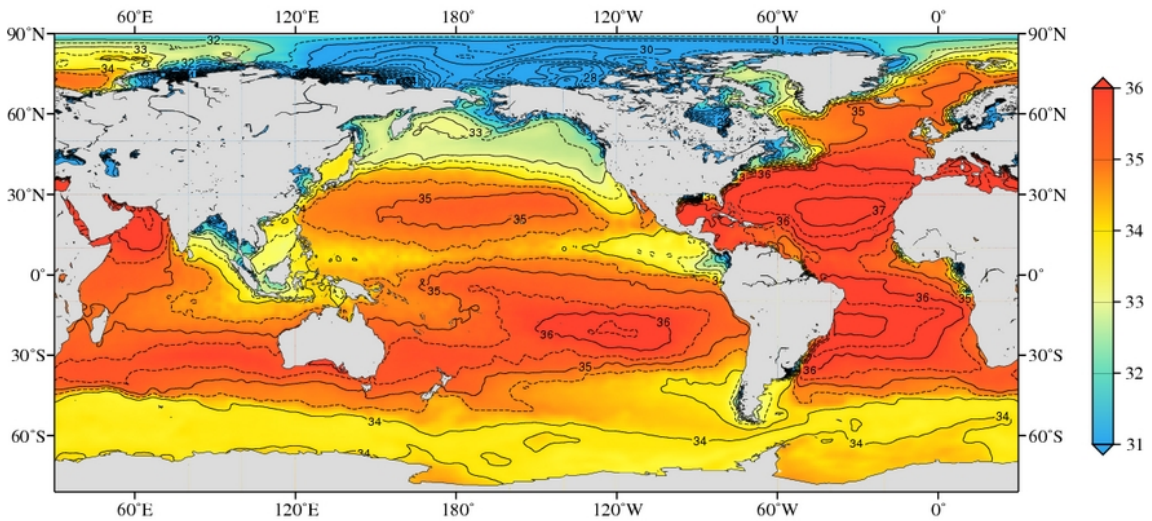


Figure 3.2: 1955-2012 mean sea surface salinity (source: World Ocean Atlas). Although circulation features appear, it mostly reflects the surface water budget (evaporation minus precipitation).

Exercise: Application of the water and salt conservation to a semi-enclosed basin with a two-way flow at its outer strait. The Mediterranean Sea is a semi-enclosed sea connected to the Atlantic Ocean by a two-way flow at Gibraltar Strait. We know that the salinities of the incoming and outgoing waters are respectively $S_i = 36.5\text{‰}$ and $S_o = 38.5\text{‰}$ and that the average net surface water flux (precipitation plus river runoff minus evaporation) within the basin is $Q_s = -0.05 \times 10^6 \text{m}^3/\text{s} = -0.05\text{Sv}$, the Sverdrup (Sv) being a common unit in oceanography. Deduce the incoming and outgoing water fluxes Q_i and Q_o .

Solution: $Q_i = +0.96\text{Sv}$ and $Q_o = -0.91\text{Sv}$, which ensures that the Mediterranean sea mass is conserved (the sea level does not fall down forever) and so is its salt (the water does not become saltier forever). This explains why fluxes between basins are generally two-way in order to equilibrate both the mass and salt budgets.

3.3 Hydrography at depth

The gyres have a relatively deep hydrographic signature, down to $\sim 1000\text{m}$ depth, with blobs of warm (respectively cold) waters within subtropical (respectively subpolar) gyres (Fig.3.3). Those blobs indicate isothermal depth anomalies opposite to the sea level. They can be interpreted in light of Margules's relation.

Exercise: derive Margules's relation for a typical subtropical gyre. We assume that the ocean

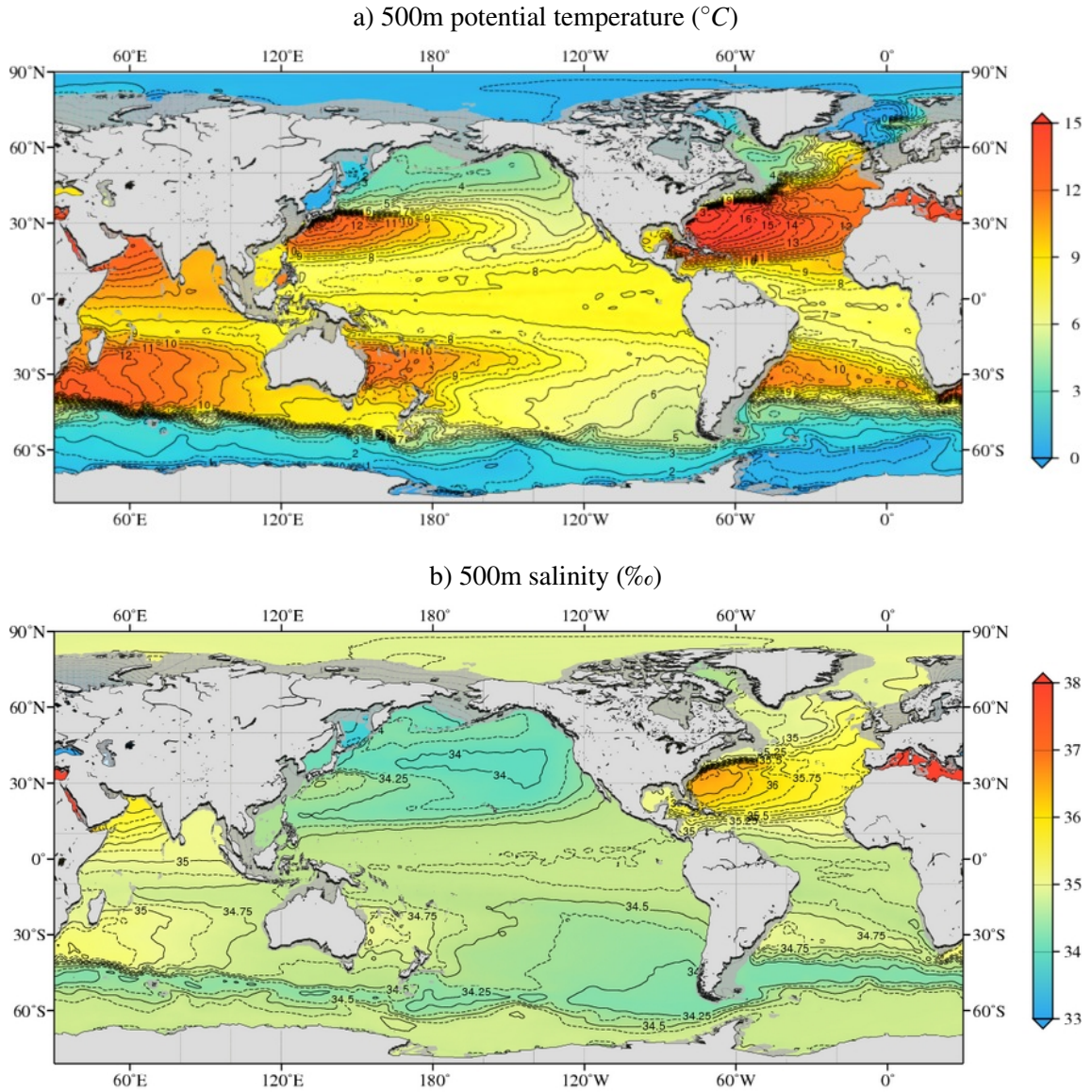


Figure 3.3: 1955-2012 mean potential temperature and salinity at 500m depth (source: World Ocean Atlas). The gyre circulation is evident on both fields.

is a two-layer fluid of respective densities $\rho_1 = 1022\text{kg/m}^3$ and $\rho_2 = 1027\text{kg/m}^3$ with only the upper layer in motion, the lower layer being assumed at rest. The zonal sea level anomaly between the center and the eastern edge of the subtropical gyre is $\Delta\eta_1 = -1\text{m}$ over the basin width of $L = 5000\text{km}$. Deduce the meridional geostrophic velocity in the upper layer and the slope of the interface η_2 between both layers that ensures the lower layer stays at rest.

Solution: $v_{g1} = -2.7\text{cm/s}$ and $\Delta\eta_2 = \frac{\rho_1}{\rho_1 - \rho_2}\Delta\eta_1 = +204\text{m}$. The relatively weak southward velocity illustrates that the gyre circulation is weak in the interior ocean and results from time averaging. As illustrated before, it does not stand out clearly from instantaneous velocity fields dominated by much more energetic mesoscale dynamics. The steep interface slope permits to interpret the presence of blobs with a structure symmetric to sea level down to $\sim 1000\text{m}$ depth.

Going deeper in the water column (Fig.3.4) water masses are more homogeneous, and generally much colder and fresher than in the surface. We deduce from the thermal wind relation that the deep ocean is very quiescent compared to the surface. The cold and fresh deep water is an

indication of their formation at high latitude, in so-called "deep convection" areas. Hence most of the oceanic volume has the physical properties and is formed at high latitude environments, which stresses their importance for the global circulation.

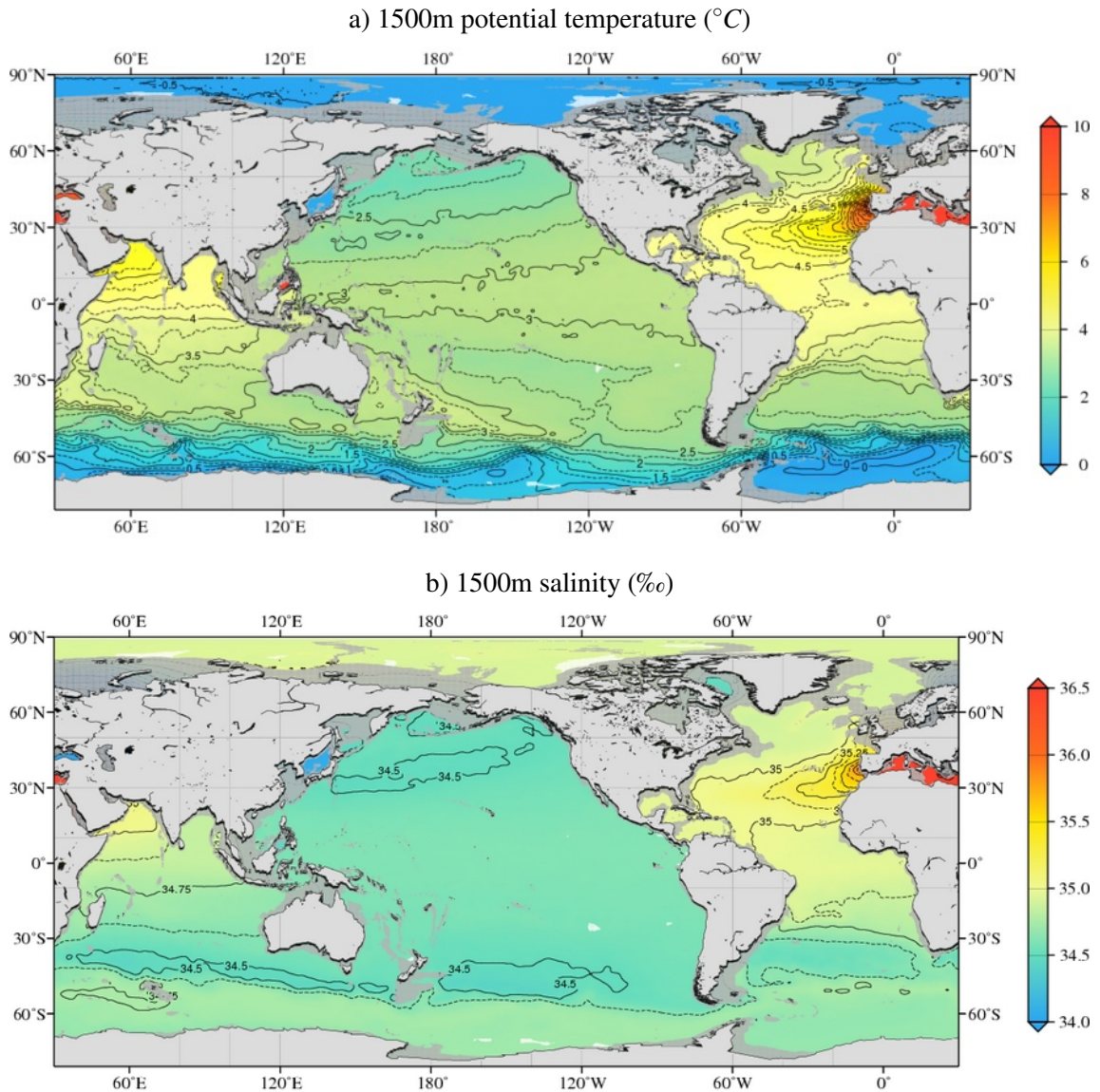


Figure 3.4: 1955-2012 mean potential temperature and salinity at 1500m depth (source: World Ocean Atlas). Weak large-scale gradients appear, related to basin-scale imbalances or the thermohaline circulation activated at high latitudes.

3.4 The vertical hydrographic structure

The vertical hydrographic structure generally separates three layers (Fig.3.5). A well-mixed surface boundary layer is in direct interaction with the atmosphere: it is the mixed layer. It is homogenized by surface heat and momentum fluxes. An intense gradient layer isolates the mixed layer from below. It is the pycnocline (literally: the density gradient), which generally corresponds to the thermocline (literally: the thermal gradient) and more rarely to the halocline (literally: the saline gradient). Below is a much more homogeneous and less energetic layer named the

interior ocean. Its hydrographic properties suggest that those water masses are formed at high latitudes. This is confirmed by subpolar hydrographic profiles which can be homogeneous down to the ocean bottom: in this case there is no pycnocline and the mixed layer is equal to the interior ocean (Fig.3.5). The process of storage of water masses from the mixed layer below the thermocline is named subduction.

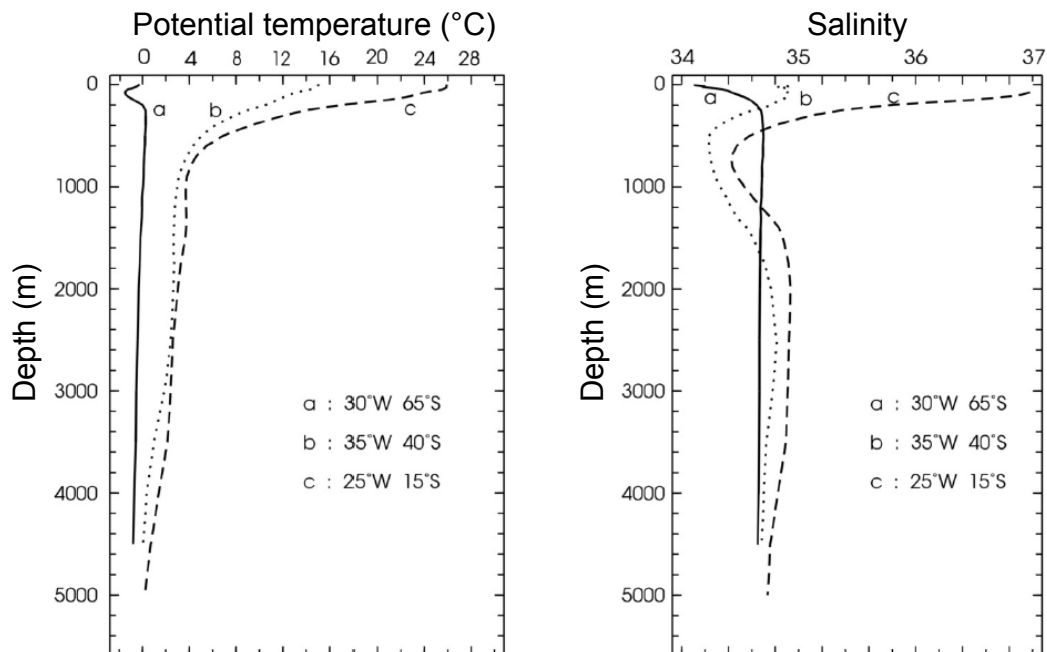


Figure 3.5: Vertical hydrological profile as a function of latitude in the Southern Atlantic region (Benjamin Ménérier's lecture). The lower the latitude, the higher the vertical stratification.

The mixed layer experiences intense seasonal transformations (Fig.3.6). It is shallow in summer under the action of solar warming. It then cools down and deepens in fall by entrainment of underlying waters under the action of both cooling and wind stress. It reaches a maximum depth in the late winter, at the end of the heat loss period. This annual maximum depth is of paramount importance because it determines the depth of the water column which is ventilated and interacts yearly with the atmosphere. It also drives subduction, which occurs during spring when the mixed layer shoals under the effect of solar warming. In spring, a fraction of the winter mixed layer is detrained (meaning isolated) from the mixed layer and can remain below the thermocline for years to millennia.

Exercise: what air-sea heat flux Q_0 (in J/m^2) is required to cool down a mixed layer of $h = 50m$ depth by $1^\circ C$? By how many degrees would this flux heat a surface atmospheric layer of the same height? What are the consequences for oceanic static stability? The heat capacities at constant pressure are respectively $c_w = 3993J/K/kg$ and $c_a = 1005J/K/kg$, with respective densities of $\rho_w = 1025kg/m^3$ and $\rho_a = 1.2kg/m^3$.

Solution: $Q_0 = 1 \times h \times \rho_w \times c_w = 204.6MJ/m^2$ and $\Delta T_a = \frac{Q_0}{h \times \rho_a \times c_a} = +3396.4^\circ C$. We conclude that it is mostly the large difference in densities between sea and air (and partly the higher heat capacity per unit mass) that explains the relative decoupling between both components and why the ocean is a slowly-evolving component of the climate system. In the ocean, a surface cooling induces a static instability at the basis of the mixed layer, where colder waters are above warmer waters. This triggers oceanic convection towards the bottom, which deepens the mixed

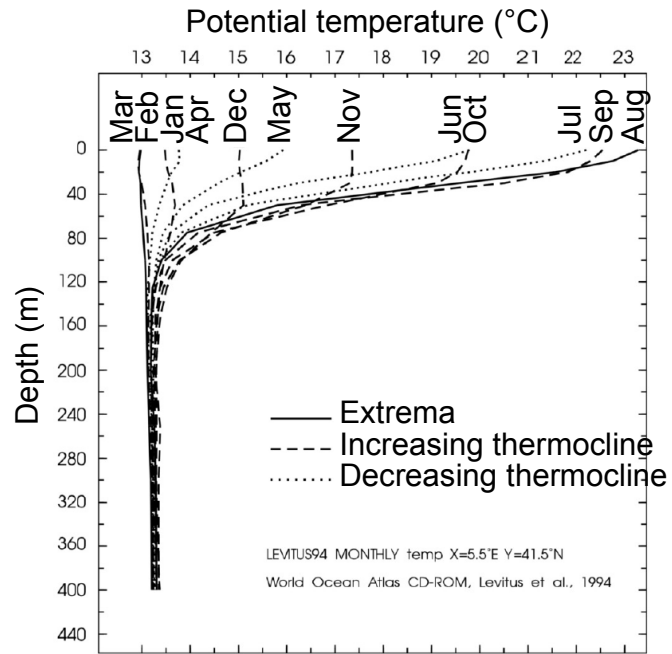


Figure 3.6: Seasonal cycle of the vertical hydrological profile in a deep convection region of the Mediterranean Sea (source: Levitus 1994 and Benjamin Ménétrier's lecture). We can identify the winter deep water formation by the homogenization of the water column resulting from surface cooling.

layer.

4 Fluxes at the air-sea interface and climatic relevance

The ocean exchanges mass, energy and momentum at its interface with the atmosphere. Those fluxes can be decomposed into radiative and turbulent contributions, all counted positive toward the ocean in the following. The surface energy imbalance is equilibrated by the ocean circulation, which is hence a key component of the climate system.

4.1 The surface heat fluxes

4.1.1 Radiative heat fluxes

Radiative heat fluxes can be decomposed between the shortwave incoming solar heat flux, partially reflected by the ocean surface (Q_{SW}) and the longwave radiative fluxes coming downward from the atmosphere and upward from the ocean (Q_{LW}). Indeed, because of the large temperature difference between the Sun surface and the ocean-atmosphere, their radiative emission spectra are relatively well separated.

Solar radiation is the main source of energy for the ocean (Fig.4.1). Remarkably, the ocean has a very low and relatively constant albedo $\alpha \sim 0.06$ (except in the presence of sea ice), meaning that most of the incoming surface solar radiation is absorbed by the ocean. Also, because of the high light absorption capacity of sea water, most of this solar warming is concentrated within the first meters of the water column (exponential decay of typically a few meters). Solar radiation depends mostly on the solar zenith angle V_s and on the proportion that is transmitted by the atmosphere T_a , which is mostly a function of cloudiness. It can be expressed as:

$$Q_{SW} = F_s \cos(V_s) T_a (1 - \alpha)$$

with $F_s = 1361 \text{ W/m}^2$ the solar constant.

The distribution of Q_{SW} is dominated by its latitudinal dependence, but it is also modulated by atmospheric cloudiness (Fig.4.1). This is why a minimum is visible a few degrees north of the Equator, at the mean location of the ITCZ. Also, a stronger meridional gradient than expected from the zenith angle is present at mid-latitudes: this is due to the high cloudiness at high-latitudes.

The longwave radiation is the resultant from the downward atmospheric and upward oceanic contributions (Fig.4.1). They can both be modelled as grey bodies emitting a radiative heat flux which is function of their temperature:

$$Q_{LW} = (1 - \alpha_{LW}) \epsilon_a \sigma T_a^4 - \epsilon_o \sigma SST^4$$

with $\sigma = 5.67 \times 10^{-8} \text{ W/m}^2/\text{K}^4$ the Stephan-Boltzmann constant, $\alpha_{LW} = 0.045$ the oceanic longwave albedo (also weak and relatively constant), ϵ_a (very variable) and $\epsilon_o = 0.97$ the respective emissivities of both fluids.

Globally, the ocean loses heat by longwave radiation (Fig.4.1) because the SST is on average higher than T_a (Fig.4.2). Q_{LW} is relatively homogeneous spatially. This is due to the compensation between the incoming atmospheric and outgoing oceanic radiations. When the ocean is warmer and emits more longwave radiation, atmospheric temperature, humidity and cloudiness are also larger which feeds back negatively on Q_{LW} . We note however a maximum negative Q_{LW} in subtropical regions where cloudiness and atmospheric humidity are low.

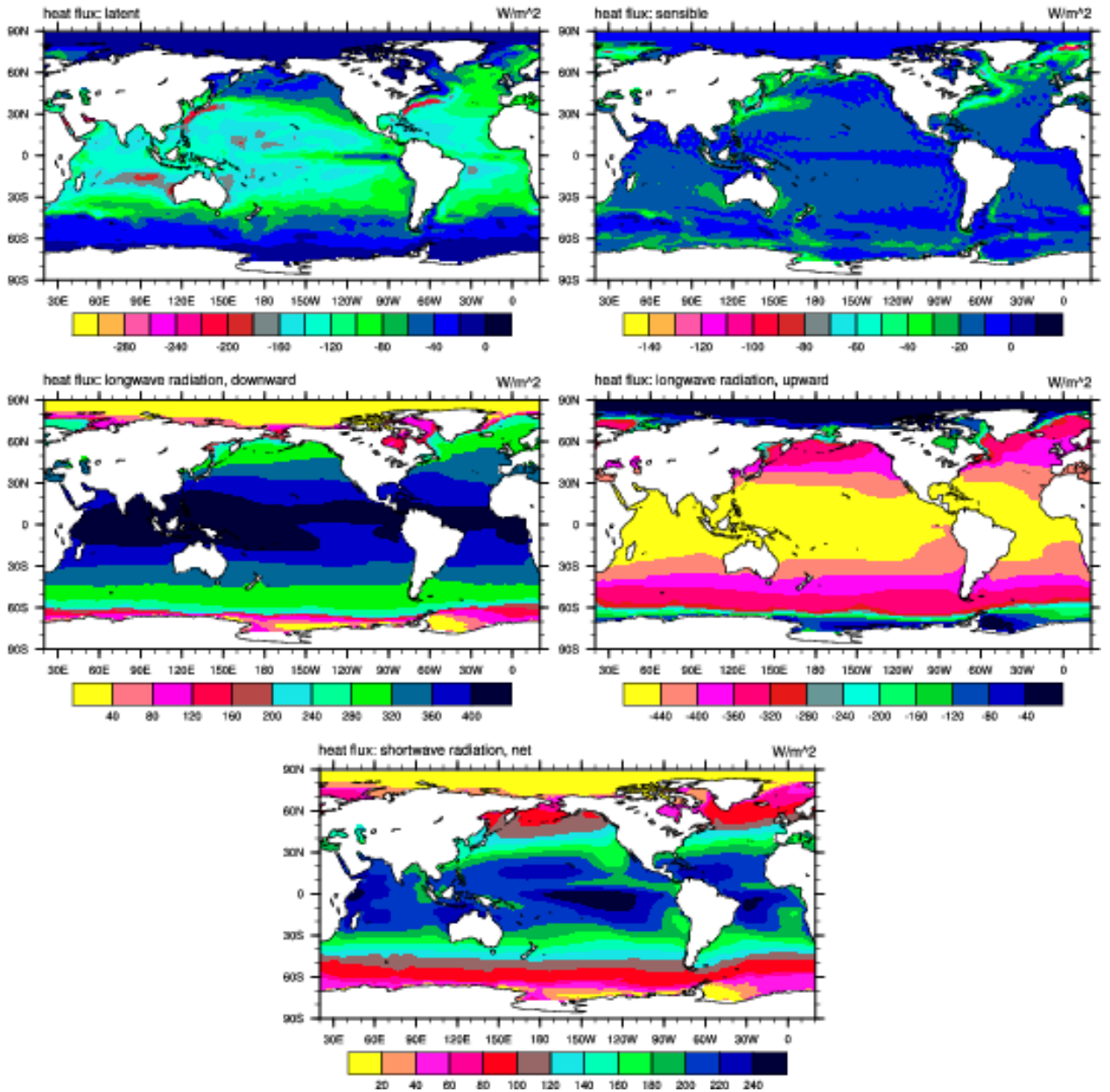


Figure 4.1: 1984–2006 average latent, sensible, downward and upward longwave and net shortwave heat fluxes at the air-sea interface deduced from an atmospheric reanalysis (source: CORE2/NCAR). The shortwave heat gain and latent heat loss dominate the balance.

4.1.2 Turbulent heat fluxes

In a very thin surface diffusive layer less than 1mm thick at the air-sea interface, called the "cool skin" in the ocean, sensible heat (and water vapor in the atmosphere) are exchanged by both fluids by conduction. A strong temperature gradient exists there which is why SST measured by satellite (at a few μm depth) is systematically lower than the in situ measured SST (between $\sim 0.5 - 5\text{m}$). However, this conductive layer is hardly measurable and outside of it sensible heat and water vapor exchanges are dominated by turbulent fluxes by atmospheric eddies. Namely, it is the turbulent vertical flux that dominates both exchanges: $\overline{w'\theta'}$ for sensible heat flux and $\overline{w'q'}$

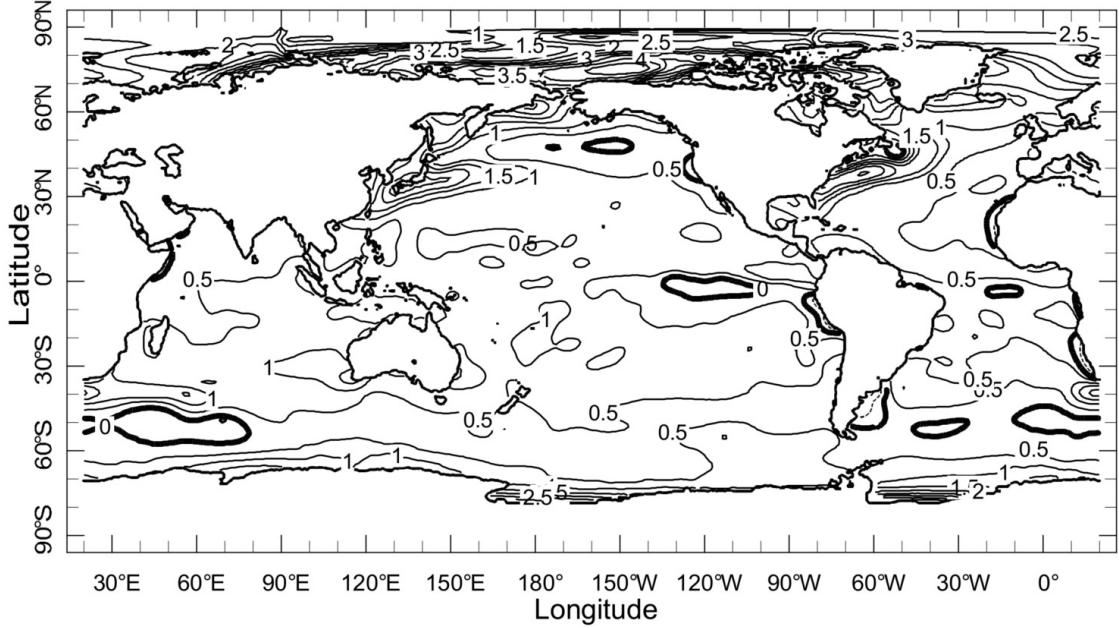


Figure 4.2: Annual mean ocean-atmosphere surface temperature difference in $^{\circ}\text{C}$ (source: Benjamin Ménétrier's lecture).

for water vapor flux with w , θ and q the atmospheric vertical velocity, potential temperature and specific humidity, the prime and overbar denoting anomaly and mean from Reynolds averaging (usually time averaging), e.g. $\theta = \bar{\theta} + \theta'$. Both determine two fundamental heat fluxes at the air-sea interface: the sensible Q_S and latent Q_L heat fluxes (Fig.4.1), the latter resulting from surface evaporation. Those turbulent transports are themselves hardly measurable, so that they are usually estimated from so-called "Bulk aerodynamic formulas" which relate them to the average properties of the air-sea interface. Those formulas derive from the Monin-Obukhov Similarity Theory and are expressed as follows:

$$Q_S = -\rho_a c_a C_\theta |\mathbf{U}(10\text{m})| (SST - \theta_a(2m))$$

and

$$\begin{aligned} Q_L &= -\rho_a L_v C_q |\mathbf{U}(10\text{m})| (q_s - q(2m)) \\ &= -\rho_a L_v C_q |\mathbf{U}(10\text{m})| (0.98q^*(P_0, SST) - q(2m)) \end{aligned}$$

with $L_v = 2.26\text{MJ/kg}$ the latent heat of evaporation, $|\mathbf{U}(10\text{m})|$ the wind module at 10m height, $\theta_a(2m)$ and $q(2m)$ the potential temperature and specific humidity at 2m height, $q_s = 0.98q^*(P_0, SST)$ the specific humidity at surface which is equal to the saturating humidity (the factor 0.98 is due to ocean salinity) and C_θ and C_q empirical transfer coefficient depending on the wind, surface roughness and atmospheric stability. Intuitively, those formulas state that stronger winds will increase sensible and latent heat fluxes, and that the larger the near-surface gradient of temperature and humidity, the higher the respective heat fluxes.

Q_S is on average slightly negative (Fig.4.1) because generally $SST > T_{2m}$ and because turbulent heat transfers are more efficient for warm SST due to atmospheric convection. In addition, we identify regions of strong heat loss at the western boundary of subtropical gyres, where intense cold wind blows over a warm SST. Despite its negative feedback which always tends to reduce air-sea temperature differences, Q_S is the weakest contribution to the surface heat budget.

On the contrary, Q_L is systematically negative and can be very intense due to the large latent heat of evaporation and an average surface evaporation of $E = -1.2\text{m/year}$ (Fig.4.1). Hence it

is the major oceanic heat loss equilibrating the solar radiation Q_{SW} . Similarly to Q_S , the latent heat loss is maximum where strong cold winds blow above warm SSTs, as in the western edge of subtropical gyres. It is also high at tropical latitudes below the trade wind jets. In the ITCZ, Q_L is weak because of weak winds despite warm SSTs, and reversely in the Southern Ocean where Q_L is weak because of cold SSTs despite strong winds.

4.1.3 Total net heat flux

The total net heat flux Q_0 (also written Q_{net} or Q_{tot}) is:

$$Q_0 = Q_{SW} + Q_{LW} + Q_S + Q_L$$

As in the atmosphere, it is positive at low latitudes and negative at high latitudes (Fig.4.3), meaning that ocean circulation transports heat poleward to balance the oceanic heat budget, hence its climatic importance. Globally, Q_0 is dominated by the balance between solar radiation ($Q_{SW} = +150W/m^2$) and latent heat loss ($Q_L = -90W/m^2$), with a smaller contribution of longwave radiation ($Q_{LW} = -50W/m^2$), the sensible heat flux being an order of magnitude smaller ($Q_S = -10W/m^2$). The net energy imbalance at the air-sea interface resulting from anthropogenic climate change is $Q_0 \sim +0.7W/m^2$, hence a tiny residual of very large individual contributions. This illustrates the difficulty to measure the surface energy imbalance, which is actually estimated indirectly from variations in the global ocean heat content. It also shows that to a very good approximation, the heat budget of individual components of the climate system is closed.

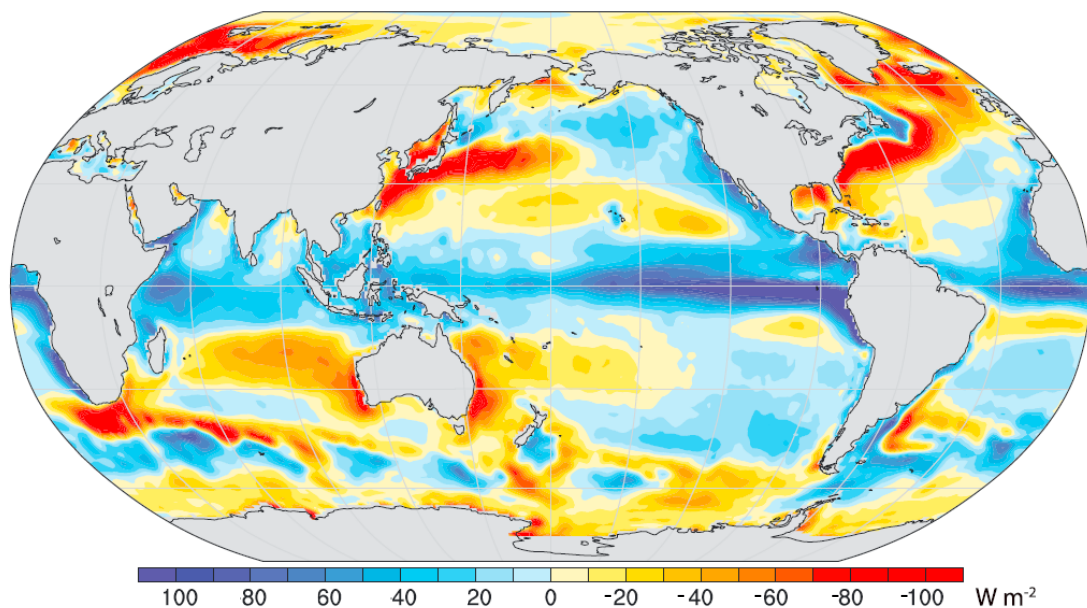


Figure 4.3: 2000–2014 average total net air-sea heat flux deduced from the atmospheric energy budget (source: Trenberth and Fasullo 2017, caution color code reversed). The global mean flux must be balanced, so that the low-latitude ocean heat gain is equal to the high-latitude and western boundary heat loss.

Exercise: qualitatively, what negative feedbacks in the air-sea fluxes occur if Q_{SW} increases? What if the SST increases?

Solution: the increase in Q_{SW} will induce a negative feedback of all three other air-sea heat fluxes through its impact on SST. Indeed, a warmer SST will cause larger upward Q_{LW} (grey body law), more Q_S toward the atmosphere ($T_a - SST$ more negative) and higher Q_L (higher q_s^ at higher*

temperature). The increase in SST will similarly increase these three heat fluxes, which will also act as a negative feedback. In addition, increased atmospheric convection above a warm SST will increase cloudiness and hence reduce Q_{SW} . In both case, a new and warmer climate balance will be reached which closes the surface heat budget.

4.2 The surface momentum fluxes

Similarly to sensible and latent air-sea heat fluxes, surface momentum fluxes are dominated by vertical turbulent motions of atmospheric eddies (the eddy flux $\overline{w'u_p}$). They are very difficult to measure directly and hence are approximated by the following "Bulk aerodynamic formula":

$$\tau_0 = \rho_a C_d |\mathbf{U}(10\text{m}) - \mathbf{u}_o| (\mathbf{U}(10\text{m}) - \mathbf{u}_o)$$

with τ_0 surface wind stress, C_d the momentum drag coefficient, \mathbf{u}_o surface ocean currents, or neglecting the latter:

$$\tau_0 = \rho_a C_d |\mathbf{U}(10\text{m})| \mathbf{U}(10\text{m})$$

τ_0 is largely dominated by the wind magnitude (Fig.4.4), although surface roughness and atmospheric stability also intervene in C_d . Hence it is maximum at mid latitude below Westerlies, especially in the Southern Ocean because of the absence of continental barriers. It also reaches a relative maximum at $\sim 15^\circ$ of latitude, below the trade wind jet.

4.3 The surface water fluxes

Surface water fluxes are dominated by evaporation, precipitation and river runoff (Fig.4.5). The ocean loses on average 0.1m/year of water to the atmosphere by the exceedance of evaporation ($E = -1.2\text{m/year}$) over precipitation ($P = +1.1\text{m/year}$), which is returned to the ocean by the coastal river runoffs ($R = +0.1\text{m/year}$). Minor contributions can add up to this budget: glacier and ice sheet (including ice shelves and icebergs) melting which contribute to $\sim 2/3$ of the anthropogenetic sea level change ($\sim +2\text{mm/year}$), sea ice formation and melting and groundwater discharges. Evaporation is exactly proportional to Q_L and hence maximum in the subtropics, especially at their western boundaries, and minimum at high latitudes and along the ITCZ. Precipitation over the sea is particularly challenging to observe. However atmospheric reanalyses (which assimilate observations but also contain model information) suggest a general pattern opposite to that of evaporation with maximum values in the ITCZ and at high latitudes, and minimum values in the Subtropics and at their eastern edges. River runoff is very localized at the mouth of the largest rivers, most of which are located in the Tropics. It does not occur exclusively at surface, as estuarine processes can distribute them vertically over typically a few tens of meters.

4.4 The oceanic contribution to the Earth's heat balance

We have seen that the oceanic heat capacity is several thousand times larger than that of the atmosphere. It is actually by far the largest among components of the climate system (Fig.4.6), so that $\sim 90\%$ of the global warming has been absorbed by the ocean. It corresponds to an air-sea energy imbalance of $Q_0 \sim +0.7\text{W/m}^2$ out of a total (top of the atmosphere) of $Q_{TOA} \sim +0.8\text{W/m}^2$ for the climate system. $2/3$ of it is believed to have been absorbed by the top 700m , although little is known about the ocean heat content below 2000m depth. Hence the ocean acts as a climate buffer, which explains why the surface anthropogenetic warming is weaker by a factor ~ 1.5 over the sea than over the land (Fig.1.10a).

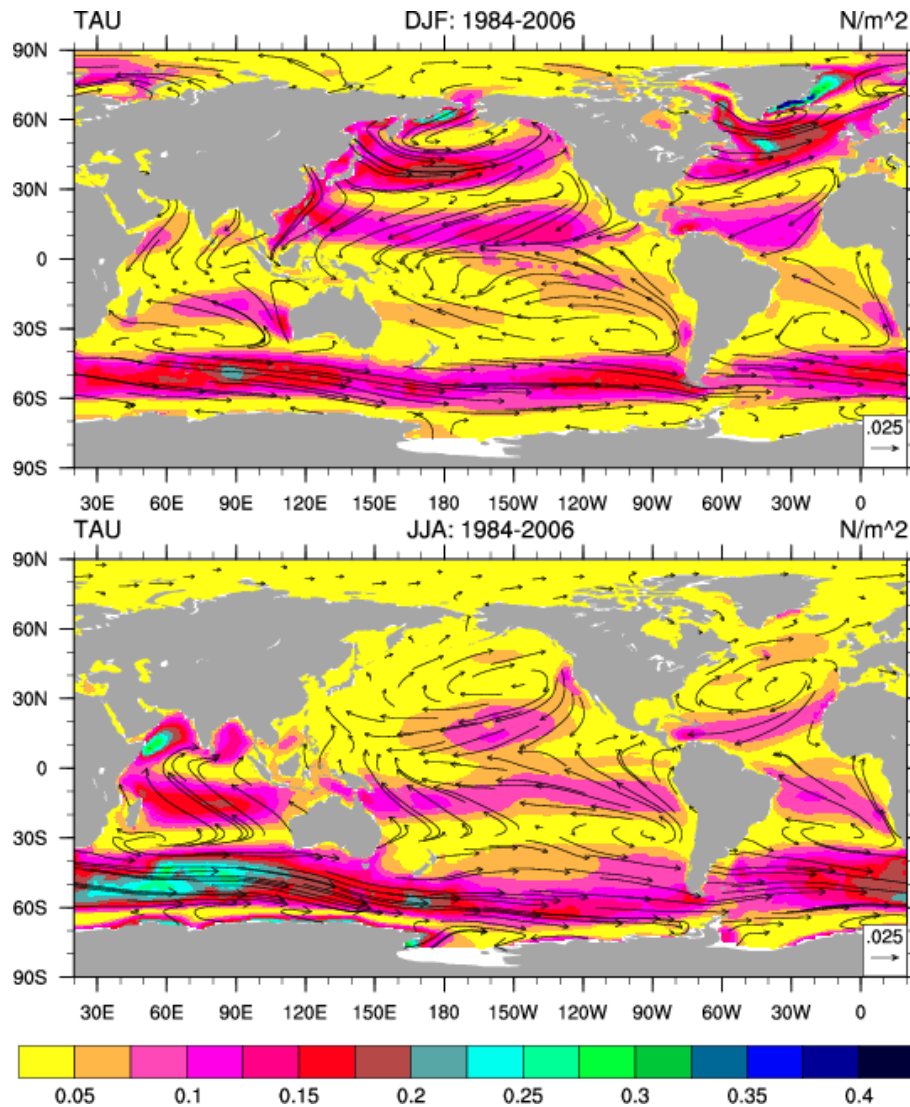


Figure 4.4: 1984–2006 average momentum flux at the air-sea interface (wind stress) for the boreal and austral winters deduced from an atmospheric reanalysis (source: CORE2/NCAR). The mid-latitude westerlies and the tropical trade winds stand out.

Meridionally, the ocean contributes to $\sim 1/3$ of the poleward heat transfer, the remaining being provided by the atmosphere, both regulating the global climate (Fig.4.7). The oceanic contribution is highest and dominates in the Tropics, whereas it is much weaker at high latitudes. Both the horizontal gyre circulation and the overturning thermohaline circulation participate to this meridional heat transport. Subtropical (respectively subpolar) gyres advect warm (respectively cold) western boundary waters poleward (respectively equatorward) and return colder (respectively warmer) interior waters equatorward (respectively poleward), which causes a net poleward heat transport. The meridional overturning (or thermohaline) circulation, activated by density gradients in the deep ocean, generally transports warm upper waters poleward and cold lower waters equatorward, with the notable exception of the South Atlantic Ocean (Fig.4.7). The overturning circulation is expected to weaken in the future due to reduced deep convection under warming and increased freshwater fluxes at high latitudes. Some modelling evidence suggest that specific gyre circulations could abruptly weaken in the future with possible strong climatic implications.

Finally, the ocean also has a key climatic role in its storage of $\sim 1/4$ of anthropogenic CO_2

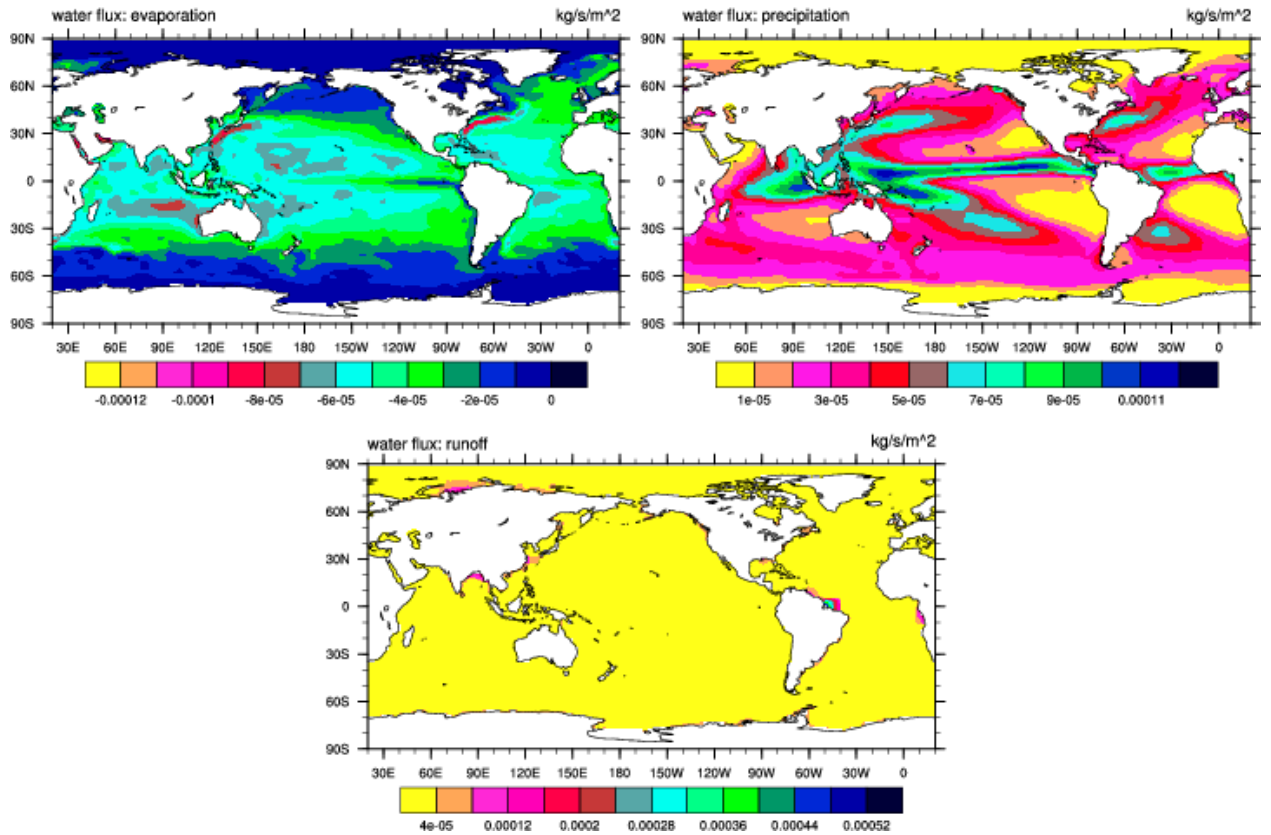


Figure 4.5: 1984–2006 average evaporation, precipitation and river runoff at the air-sea interface deduced from an atmospheric reanalysis (source: CORE2/NCAR). Evaporation occurs mostly in the Subtropics, precipitation along the ITCZ and runoff is very coastal.

emissions (Fig.4.8), hence reducing the atmospheric radiative warming. Although this CO_2 uptake is poorly known and only indirectly estimated from evolutions of the oceanic carbon inventory, it is believed to occur preferentially through physical dissolution of CO_2 into carbonates, and not through biological uptake. This physical uptake is located above cold waters that sink, because of their large absorption capacity and their relatively low carbon content. Such waters are mostly located in the subpolar North Atlantic and in the Southern Ocean. This massive carbon uptake causes a dramatic acidification of the surface ocean, with potentially dramatic consequences for marine ecosystems.

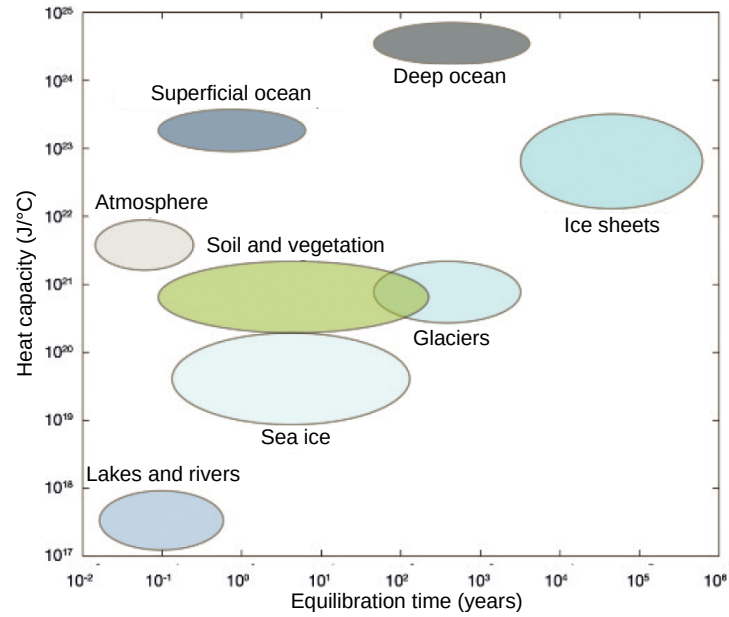


Figure 4.6: Simplified diagram of the heat capacity and equilibration time of the main climate components (source: de Lavergne 2018). The ocean stands out as the main heat reservoir with a relatively short response time.

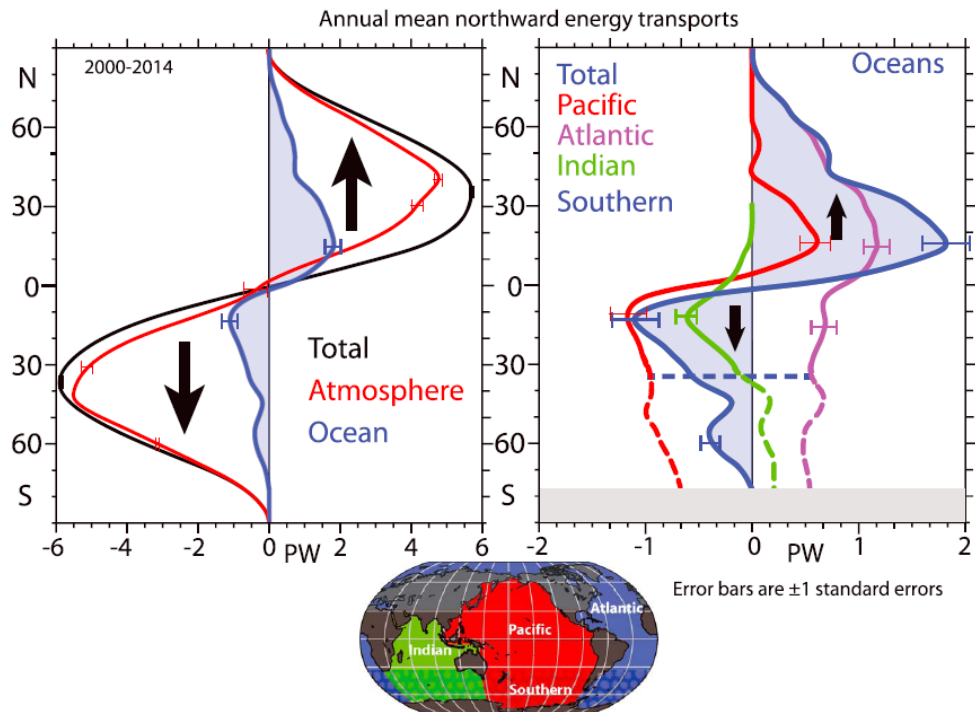


Figure 4.7: 2000–2014 average meridional heat transport as a function of latitude for the atmosphere and ocean, and for the main oceanic basins (source: Trenberth and Fasullo 2017). The atmosphere dominates except in the Tropics, and the Atlantic and Pacific Oceans have the largest contributions respectively for the Northern and Southern Hemispheres.

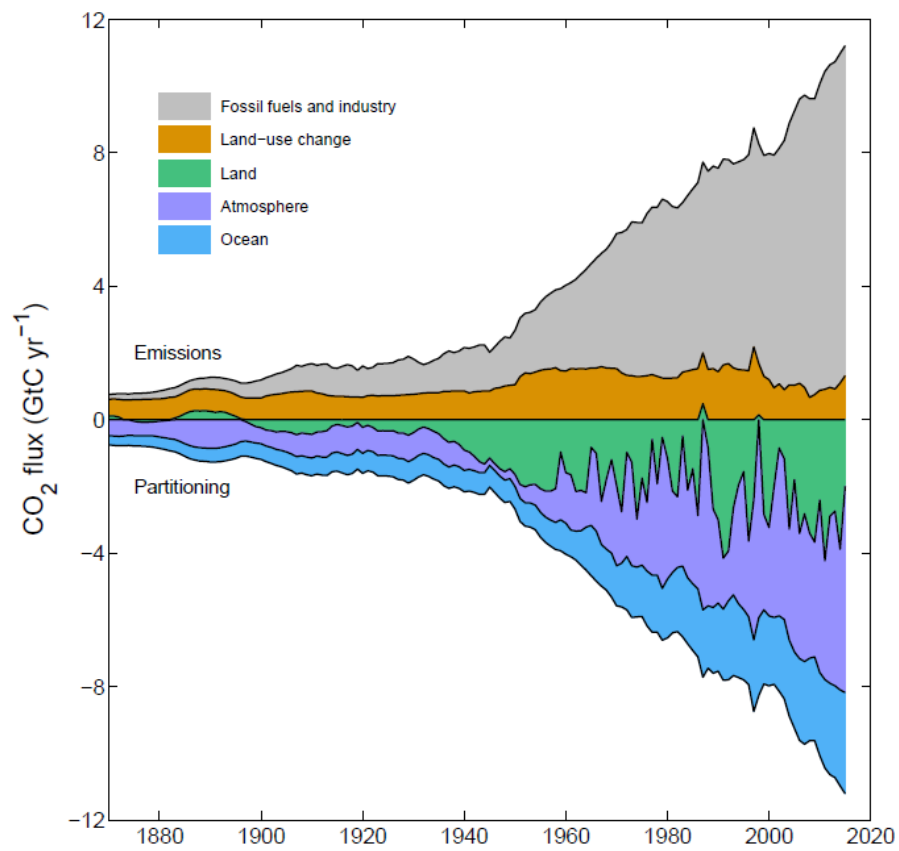


Figure 4.8: Inventory of the annual emission and storage rate of CO_2 (source: Le Quéré et al 2016). The ocean has contributed to $\sim 1/4$ of the total storage of anthropogenic CO_2 .